9 The Slave-Boson Approach to Correlated Fermions

Raymond Frésard
Laboratoire CRISMAT, UMR CNRS-ENSICAEN 6508
6, Bld. Maréchal Juin, 14050 Caen CEDEX 4 , France

Contents

1 Introduction **2**

2 Slave-boson representations **4**
2.1 Barnes's representation 4
2.2 Kotliar and Ruckenstein representation 6
2.3 Spin-rotation-invariant representation 7
2.4 Multi-band systems 8

3 Gauge symmetry and radial slave-boson fields **8**

4 Saddle-point approximations **10**
4.1 Saddle-point approximation to the Barnes representation 10
4.2 Saddle-point approximation to the Kotliar and Ruckenstein representation . . . 12
4.3 Saddle-point approximation to the multi-band Hubbard model 15
4.4 A concrete example 19
4.5 Magnetic order in the Anderson lattice model 22

5 Fluctuation corrections to the saddle-point approximation: SRI representation of the Hubbard model **23**
5.1 Magnetic and striped phases 25

6 Extended Hubbard model **26**
6.1 Saddle-point approximation to the extended Hubbard model 26
6.2 Landau parameters 27

7 Summary **30**

E. Pavarini, E. Koch, and P. Coleman (eds.)
Many-Body Physics: From Kondo to Hubbard
Modeling and Simulation Vol. 5
Forschungszentrum Jülich, 2015, ISBN 978-3-95806-074-6
http://www.cond-mat.de/events/correl15

1 Introduction

The immense and steadily increasing field of strongly correlated electrons has emerged as a central theme of many-body physics over the past three decades (for a review see [1]). Among them, the so-called heavy-fermion metallic compounds [2] and cuprate superconductors [3] have received particular attention. It is acknowledged that fully accounting for their properties is a challenging task, but it is believed that their key properties are embodied in model Hamiltonians, such as the Anderson or Kondo lattice models in the former case, and in the Hubbard model or possibly the t-J-model in the latter one [4]. The difficulty in solving these models is rooted in the fact that conventional many-body perturbation theory (including infinite resummations), does not work in these cases. This failure is obvious in lattice models with on-site repulsion U exceeding the band width D.

Take the Hubbard model with large on-site repulsion U, where each lattice site can either be empty (state $|0\rangle$), singly occupied ($|\uparrow\rangle\,, |\downarrow\rangle$), or doubly occupied ($|2\rangle$). The dynamics of an electron will be very different according to whether it resides on a singly or doubly occupied site. For large U, the doubly occupied states will be pushed far up in energy and will only marginally contribute to the low-energy physics. This leads effectively to a projection of the Hilbert space onto a subspace devoid of doubly occupied states. It turns out to be difficult to effect the projection within conventional many-body theory, as was realized early on in the context of the magnetic impurity problem. Indeed, this difficulty is at the heart of the single-impurity Kondo problem, for which a sound physical picture and quantitative analytical and numerical methods of solution have been developed over a period of 40 years [5]. We will discuss impurity models briefly in a later section. More details can be found in the review [6].

A powerful technique for describing the projection in Hilbert space is the method of auxiliary particles (slave bosons, pseudofermions [7–12]): One assigns an auxiliary field or particle to each of the four states $|0\rangle\,, |\downarrow\rangle\,, |\uparrow\rangle\,, |2\rangle$ at a given lattice site (considering one strongly correlated orbital per site). The Fermi character of the electrons requires that two of the auxiliary particles are fermions, e.g., the ones representing $|\downarrow\rangle\,, |\uparrow\rangle$ and the remaining two are bosons. Introducing new particles for the states $|0\rangle\,, |2\rangle$ allows one to express the projection to the Hilbert space of states without double occupancy as $n_0 + n_\uparrow + n_\downarrow = 1$, where n_α are the occupation numbers of the states $|\alpha\rangle$; i.e., each lattice site is either empty or singly occupied. There are various ways of defining auxiliary particles for a given problem. It is wise to choose the one that is best adapted to the physical properties of the system.

Compared to alternative ways of performing the projection, the auxiliary-particle method has the advantage of allowing one to use the machinery of quantum field theory, i.e. Wick's theorem, diagrammatic perturbation theory and infinite resummations of diagrams, provided the constraint can be incorporated in a satisfactory way.

Historically, auxiliary particle representations were first introduced in the context of spin models. Spin operators may be represented by Bose operators (Holstein-Primakoff [7], Schwinger [8]) or in the case of spin 1/2 (and with additional complications for higher spins as well) by Fermi operators (Abrikosov [9], Coqblin-Schrieffer [10]). Electron operators necessarily in-

volve a combination of auxiliary fermion and boson operators. The simplest such representation was proposed for the Anderson impurity problem by Barnes [11], and for lattice problems by Coleman [12]. A more complex representation of electron operators, incorporating the result of the Gutzwiller approximation [13] on the slave-boson saddle-point approximation level was developed by Kotliar and Ruckenstein [14]. Generalizations of the latter to manifestly spin-rotation invariant form [15, 16] and to particle-hole and spin rotation invariant form [16] have also been proposed. Generalizations to multi-band Hubbard models have been introduced as well [17–20].

Quite generally, auxiliary particle theories have to deal with two problems: the treatment of the constraint and the approximate description of the dynamics. An accurate control of the constraint alone does not yet make a good theory! In fact, the latest attempts suggest that the price to pay to exactly implement constraints is to have to diagonalize the many-body Hamiltonian matrix [21, 22].

Besides, the effect of strong Coulomb interaction in systems with orbital degeneracy plays a prominent role. Such a situation is realized in almost all transition metals and transition-metal oxides. These systems contain d-electrons in cubic or trigonal environments, the crystal field can only partially lift the degeneracy of the d-bands, for instance down to two as is the case of V_2O_3 [23] or down to three for perovskites such as $LaTiO_3$. On top of high-T_c superconductivity, a whole series of application-oriented, fundamental properties of correlated electronic systems arose in recent years, in particular for transition-metal oxides. They include colossal magnetoresistance (see, e.g., [24]), transparent conducting oxides (see, e.g., [25]), high-capacitance heterostructures [26], and large thermopower (see, e.g., [27]), to quote a few. In addition, they also entail fascinating phenomena such as superconductivity at the interface of two insulators [28], peculiar magnetism in low-dimensional systems [29], high-temperature ferromagnetism in vanadate superlattices [30], all of them providing strong motivation to investigate these systems from the theory side.

Given the variety of systems and properties of interest, it is desirable to have an approximate scheme amenable to the computation of the desired quantities as functions of interaction strength and density in the thermodynamic limit. Slave-boson approaches showed a great potential toward that aim. While the solution of the Ising chain is the only example so far that could be solved exactly through slave-boson calculations [31], approximate approaches such as the self-consistent T-matrix approximation to the single-impurity Anderson model and the slave-boson saddle-point approximation to the Hubbard model have been widely used. Part of the success of the latter follows from the fact that it is variationally controlled in the large-dimensionality limit, and it is exact in the large-degeneracy limit. Further, it can be improved systematically by performing a loop-expansion around the saddle point.

In Section 2 we review the various slave-boson representations of the most prominent models. Section 3 is devoted to the gauge symmetry of the Barnes slave-boson representation of the single-impurity Anderson model and to the concept of a radial slave-boson field, which is shown in general to possess an exact, non-vanishing expectation value. The saddle-point approximation is applied to several models in Section 4. Fluctuation corrections, calculation of

the spin and charge autocorrelation functions as well as magnetic phases are addressed in Section 5. Recent applications to a Hubbard model extended by long-ranged Coulomb interactions are presented in Section 6, and the results are summarized in Section 7.

2 Slave-boson representations

The goal of a slave-boson (SB) representation is to describe an interacting fermionic system by means of an action that is bilinear in fermionic fields. In these frameworks one avoids Hubbard-Stratonovich decoupling the interaction terms, which typically shares the difficulties and limitations of perturbation theory. It necessitates introducing auxiliary fermionic fields, which will be denoted below by the doublet $\{f_\sigma\}$, and slave-boson fields, say $\{e, p, d\}$, in terms of which one needs to rewrite the physical electron operators $\{a_\sigma\}$. All of them satisfy canonical commutations. By doing so, one increases the number of degrees of freedom (DoF), implying that the auxiliary fields need to satisfy constraints to ensure a faithful representation of the original model. These constraints can be handled in the functional integral formalism [32]. A particularity of SB approaches is the apparition of radial slave boson fields: They are bosonic fields with their amplitude as sole DoF. Being phase-free, their exact expectation value may be finite in accordance with Elitzur's theorem, as discussed below.
A natural basis of the Hilbert space of electrons in a local orbital may be chosen as consisting of four states: two with single occupancy (representing a local spin $1/2$) and the empty and doubly occupied states. Forming a doublet, the singly occupied states manifestly have fermionic character, while the remaining two states have bosonic character. Below, we shall create these states out of a vacuum state $|\text{vac}\rangle$, which is annihilated by any of the above auxiliary fields. These four states may then be created by fermionic or bosonic auxiliary operators. This may be achieved in a multitude of ways. We will concentrate here on the representations introduced by Barnes for the single-impurity Anderson model [11], by Kotliar and Ruckenstein [14], and by Wölfle *et al.* for the Hubbard model [15,16], as well as an extension to multi-band systems [17].

2.1 Barnes's representation

The basic idea consists in locally decomposing the electronic excitations into spin and charge components. There are many different ways to achieve this goal. For instance, it could be reached by means of a suitable Hubbard-Stratonovich decoupling of the interaction term but would likely be limited to weak interaction. Instead, in his pioneering work, Barnes suggested representing the spin and charge degrees of freedom by fermionic and bosonic operators, respectively [11]. Being more numerous than the original (physical) operators, the auxiliary operators span a Fock space that is larger than the physical one. They therefore need to fulfill constraints for such a representation to be faithful. In fact, it can be shown that one constraint suffices. Specifically, Barnes considered the single-impurity Anderson model (SIAM):

$$H = \sum_{\vec{k}\sigma} \varepsilon_{\vec{k}}\, c^\dagger_{\vec{k}\sigma} c_{\vec{k}\sigma} + \varepsilon_f \sum_\sigma a^\dagger_\sigma a_\sigma + V \sum_{\vec{k}\sigma} \left(c^\dagger_{\vec{k}\sigma} a_\sigma + a^\dagger_\sigma c_{\vec{k}\sigma} \right) + U\, a^\dagger_\uparrow a_\uparrow a^\dagger_\downarrow a_\downarrow \,. \tag{1}$$

For the f electrons that are described by this model, the interaction strength is large and often treated in the $U \to \infty$ limit. To that aim, Barnes introduced auxiliary fermionic $\{f_\sigma\}$ and bosonic $\{e, d\}$ operators that satisfy canonical commutation relations. In terms of these, the physical electron operators a_σ read

$$a_\sigma = e^\dagger f_\sigma + \sigma f^\dagger_{-\sigma} d \ . \tag{2}$$

The a_σ operators obey the ordinary fermion anticommutation relations. Yet this property is not automatically preserved when using the representation Eq. (2), even when the fermionic and bosonic auxiliary operators obey canonical commutation relations. In addition, the constraint

$$Q \equiv e^\dagger e + \sum_\sigma f^\dagger_\sigma f_\sigma + d^\dagger d = 1 \tag{3}$$

must be satisfied. Eqs. (2-3) make for a faithful representation of the physical electron operator in the sense that both a_σ and its expression in terms of auxiliary particles Eq. (2) possess the same matrix elements in the physical Hilbert subspace with $Q = 1$. The above representation has been widely used, in particular in the $U \to \infty$ limit where the operator d (linked to double occupancy) drops out. One can implement the constraint by means of a functional integral representation. For example, for $U \to \infty$ the partition function, projected onto the $Q = 1$ subspace, reads

$$Z = \int_{-\pi/\beta}^{\pi/\beta} \frac{\beta d\lambda}{2\pi} \, \mathrm{e}^{i\beta\lambda} \int \prod_\sigma D[f_\sigma, f^\dagger_\sigma] \int \prod_{\vec{k}\sigma} D[c_{\vec{k}\sigma}, c^\dagger_{\vec{k}\sigma}] \int D[e, e^\dagger] \, \mathrm{e}^{-\int_0^\beta d\tau (\mathcal{L}_f(\tau) + \mathcal{L}_b(\tau))} \tag{4}$$

with the fermionic and bosonic Lagrangians

$$\begin{aligned} \mathcal{L}_f(\tau) &= \sum_{\vec{k}\sigma} c^\dagger_{\vec{k}\sigma}(\tau)(\partial_\tau + \varepsilon_{\vec{k}} - \mu) c_{\vec{k}\sigma}(\tau) + \sum_\sigma f^\dagger_\sigma(\tau)(\partial_\tau + \varepsilon_f - \mu + i\lambda) f_\sigma(\tau) \\ &\quad + V \sum_{\vec{k}\sigma} \left(c^\dagger_{\vec{k}\sigma}(\tau) f_\sigma(\tau) e^\dagger(\tau) + h.\,c. \right) \\ \mathcal{L}_b(\tau) &= e^\dagger(\tau)(\partial_\tau + i\lambda) e(\tau) \ . \end{aligned} \tag{5}$$

Here the role of the λ integration is to enforce the constraint. Since the latter commutes with the Hamiltonian, one single integration is sufficient, and introducing a time-dependent λ to integrate over would be superfluous. Furthermore, the fermions may be integrated out since the Lagrangian is bilinear in the fermionic fields. Remarkably, this has been achieved without decoupling the interaction term. As a matter of principle one should verify the correctness of the representation. This can be done in, e.g., the $V \to 0$ limit by carrying out all integrals. By virtue of the substitution $z = \mathrm{e}^{-i\beta\lambda}$, $\beta d\lambda = i dz/z$, the λ integral in Eq. (4) is transformed into a contour integral along the complex unit circle. Observing that this substitution implies a 2nd-order pole at $z = 0$ (i.e., at $i\lambda \to +\infty$, real), one obtains the expected result:

$$Z = 1 + 2\,\mathrm{e}^{-\beta(\varepsilon_f - \mu)} \ . \tag{6}$$

Alternatively, Eq. (4) may be viewed as the projection of the product of two non-interacting partition functions for each spin projection onto the $U = \infty$ subspace. Indeed Eq. (4) may be rewritten as:

$$Z = P \prod_{\sigma} \det \left[S_\sigma[e(\tau), \lambda] \right] . \tag{7}$$

Here, $\det \left[S_\sigma[e(\tau), \lambda] \right]$ is the fermionic determinant for one spin species involving an effective time-dependent hybridization ($Ve^\dagger(\tau)$), while the projection operator is given by

$$P = \int_{-\pi/\beta}^{\pi/\beta} \frac{\beta d\lambda}{2\pi} \, \mathrm{e}^{i\beta\lambda} \int D[e, e^\dagger] \, \mathrm{e}^{-\int_0^\beta d\tau \mathcal{L}_b(\tau)} . \tag{8}$$

Having checked that the representation is faithful is certainly satisfactory, but there is an asymmetry in the representation of charge and spin degrees of freedom. While the former can be expressed in terms of bosons, this is not the case in the latter, and may cause unnecessary errors in any approximate treatment (for details see Ref. [16]).
With this motivation Kotliar and Ruckenstein introduced a representation where spin and charge degrees of freedom may be expressed by bosons.

2.2 Kotliar and Ruckenstein representation

Kotliar and Ruckenstein (KR) extended Barnes's representation through the introduction of two additional Bose operators linked to the spin degrees of freedom, $p_\uparrow$ and $p_\downarrow$ [14]. In this approach, the physical electron operators are represented as:

$$a_\sigma = \tilde{z}_\sigma f_\sigma \quad \text{with} \quad \tilde{z}_\sigma = e^\dagger p_\sigma + p_{-\sigma}^\dagger d \, . \tag{9}$$

The first term corresponds to the transition from the singly occupied state to the empty one, and the second term to the transition from the doubly occupied state to the singly occupied one. The representation may again be seen to be faithful, under the condition that the auxiliary operators obey canonical commutation relations and satisfy constraints. They read

$$\begin{aligned} 1 &= e^\dagger e + \sum_\sigma p_\sigma^\dagger p_\sigma + d^\dagger d \\ f_\sigma^\dagger f_\sigma &= p_\sigma^\dagger p_\sigma + d^\dagger d \qquad \sigma = \uparrow, \downarrow , \end{aligned} \tag{10}$$

and need to be satisfied on each site. They may be enforced in a functional integral representation with Lagrange multipliers in a fashion analogous to the one we encountered with the Barnes representation. Moreover, the correctness of the representation may be explicitly verified in the limit $V \to 0$ through the exact evaluation of the partition function or Green's functions. This representation allows one to express the density operator ($\sum_\sigma p_\sigma^\dagger p_\sigma + 2d^\dagger d$) and the z-component of the spin operator ($\frac{1}{2} \sum_{\sigma=\pm} \sigma \, p_\sigma^\dagger p_\sigma$) in terms of bosons. These DoFs may therefore be treated on equal footing. We show in Section 2.4 how this procedure is extended to multiband models.

2.3 Spin-rotation-invariant representation

Though faithful, the Kotliar and Ruckenstein representation is not manifestly spin-rotation-invariant (SRI). Indeed, the transverse components of the spin operator may not be simply represented in terms of auxiliary operators since $S^{x(y)}$ is neither related to $\frac{1}{2}\sum_{\sigma\sigma'} f^\dagger_\sigma \tau^{x(y)}_{\sigma\sigma'} f_{\sigma'}$ nor to $\frac{1}{2}\sum_{\sigma\sigma'} p^\dagger_\sigma \tau^{x(y)}_{\sigma\sigma'} p_{\sigma'}$. Therefore fluctuations associated with the transverse modes are not treated on the same footing as the ones associated with the longitudinal mode. To overcome this shortcoming a manifestly SRI formulation has been introduced [15, 16]. In this setup, instead of using the doublet $\{p_\sigma\}$ [14] one introduces a scalar (S=0) field p_0 and a vector (S=1) field $\vec{p} = (p_x, p_y, p_z)$. The state $|\sigma\rangle = a^\dagger_\sigma|0\rangle$ may be represented in terms of them as

$$|\sigma\rangle = \sum_{\sigma'} p^\dagger_{\sigma\sigma'} f^\dagger_{\sigma'}|\text{vac}\rangle \text{ , with } \quad p^\dagger_{\sigma\sigma'} = \frac{1}{2}\sum_{\mu=0,x,y,z} p^\dagger_\mu \tau^\mu_{\sigma\sigma'} \text{ ,} \tag{11}$$

and τ^μ the Pauli matrices. The bosons p_μ obey canonical commutation relations. Again, all auxiliary operators annihilate the vacuum ($f_\sigma|\text{vac}\rangle = e|\text{vac}\rangle = \ldots|\text{vac}\rangle = 0$). With this at hand the electron operators may be written as:

$$a_\sigma = \sum_{\sigma'} f_{\sigma'} \tilde{z}_{\sigma'\sigma} \text{ , with } \quad \tilde{z}_{\sigma'\sigma} = e^\dagger p_{\sigma'\sigma} + \sigma'\sigma p^\dagger_{-\sigma,-\sigma'} d \text{ .} \tag{12}$$

The constraints that the auxiliary operators need to satisfy read

$$1 = e^\dagger e + \sum_{\mu=0,x,y,z} p^\dagger_\mu p_\mu + d^\dagger d \tag{13}$$

$$\sum_\sigma f^\dagger_\sigma f_\sigma = \sum_{\mu=0,x,y,z} p^\dagger_\mu p_\mu + 2d^\dagger d \tag{14}$$

$$\sum_{\sigma,\sigma'} f^\dagger_{\sigma'} \vec{\tau}_{\sigma\sigma'} f_\sigma = p^\dagger_0 \vec{p} + \vec{p}^{\,\dagger} p_0 - i\vec{p}^{\,\dagger} \times \vec{p} \text{ .} \tag{15}$$

The density operator n, the density of doubly occupied sites operator D, and the spin operator $\vec{S}$ may all be expressed in terms of bosons. They read

$$n = \sum_\mu p^\dagger_\mu p_\mu + 2d^\dagger d, \quad D = d^\dagger d, \quad \vec{S} = \sum_{\sigma\sigma'\sigma_1} \vec{\tau}_{\sigma\sigma'} p^\dagger_{\sigma\sigma_1} p_{\sigma_1\sigma'} \text{ .} \tag{16}$$

The latter expression is especially useful in the context of the t-J model, in particular because the spin degrees of freedom need not be expressed in terms of the original fermions. Using the above, one can tackle models of correlated electrons such as the single-impurity Anderson model, the Anderson lattice model, the t-J or the Hubbard model. However, while the spin and charge degrees of freedom have been mapped onto bosons, anomalous propagators necessarily vanish on a saddle-point level as the Lagrangian is bilinear in the fermionic fields, independent of the model. Here they are not treated on equal footing with the spin and charge degrees of freedom. This gave sufficient motivation to introduce a manifestly spin- and charge-rotation-invariant formulation [16].

2.4 Multi-band systems

A generic Hamiltonian describing the low-energy properties of systems with orbital degeneracy can be written as

$$H = \sum_{i,j,\sigma,\rho} t_{i,j}\, a^{\dagger}_{i,\rho,\sigma} a_{j,\rho,\sigma} + U \sum_{i,\rho} n_{i,\rho,\uparrow} n_{i,\rho,\downarrow} + U_2 \sum_{i,\rho' \neq \rho} n_{i,\rho,\uparrow} n_{i,\rho',\downarrow} + U_3 \sum_{i,\sigma,\rho'<\rho} n_{i,\rho,\sigma} n_{i,\rho',\sigma}\,, \quad (17)$$

where σ is a spin index for the up and down states, ρ is labeling the M bands, and $U_n \equiv U - nJ_H$. Taking J_H finite accounts for the Hund's rule coupling, which favors the formation of magnetic moments.

For this model with on-site interaction, a SB representation can be introduced. Generalizing the Kotliar and Ruckenstein representation one may rewrite any atomic state with the help of a set of pseudo-fermions $\{f_\alpha\}$ and slave bosons $\{\psi^{(m)}_{\alpha_1,...\alpha_m}\}$ $(0 \leq m \leq 2M)$. $\psi^{(m)}_{\alpha_1,...\alpha_m}$ is the SB associated with the atomic state consisting of m electrons in states $|\alpha_1, ..., \alpha_m\rangle$, where α is a composite spin and band index. By construction, it is symmetric under any permutation of two indices and 0 if any two indices are equal. The annihilation operator of a physical electron may be expressed in terms of the auxiliary particles as

$$a_\alpha = \tilde{z}_\alpha f_\alpha\,, \quad (18)$$

where $\tilde{z}_\alpha$ describes the change in the boson occupation numbers when an electron in state α is annihilated as:

$$\tilde{z}_\alpha = \sum_{m=1}^{2M} \sum_{\alpha_1 <.< \alpha_{m-1}} \psi^{\dagger(m-1)}_{\alpha_1,...,\alpha_{m-1}} \psi^{(m)}_{\alpha,\alpha_1,...,\alpha_{m-1}} \quad \alpha_i \neq \alpha\,. \quad (19)$$

The operators $\tilde{z}_\alpha$ in Eq. (19) describe the change in the slave-boson occupation as a many-channel process. Now, the redundant degrees of freedom are projected out with the constraints

$$1 = \sum_{m=0}^{2M} \sum_{\alpha_1 <.< \alpha_m} \psi^{\dagger(m)}_{\alpha_1,.,\alpha_m} \psi^{(m)}_{\alpha_1,.,\alpha_m} \quad (20)$$

$$f^{\dagger}_\alpha f_\alpha = \sum_{m=1}^{2M} \sum_{\alpha_1 <.< \alpha_{m-1}} \psi^{\dagger(m)}_{\alpha,\alpha_1,.,\alpha_{m-1}} \psi^{(m)}_{\alpha,\alpha_1,.,\alpha_{m-1}}\,. \quad (21)$$

3 Gauge symmetry and radial slave-boson fields

When representing the electron operators a_σ as $\tilde{z}_\sigma f_\sigma$, one may infer that a group of transformations will leave this expression invariant, assuming that it acts on the fields in such a way that

$$f_\sigma(\tau) \longrightarrow f_\sigma(\tau)\, \mathrm{e}^{i\phi(\tau)}\,, \quad \text{and} \quad \tilde{z}_\sigma(\tau) \longrightarrow \tilde{z}_\sigma(\tau)\, \mathrm{e}^{-i\phi(\tau)}\,. \quad (22)$$

This is indeed the case when considering the $U \to \infty$ Barnes representation for the SIAM since $\tilde{z}_\sigma$ is given by $e^{\dagger}$. This local $U(1)$ gauge symmetry was first realized by Read and Newns [33].

One may make use of it to gauge away the phase of the slave boson, which remains as a purely radial field, while the Lagrange constraint parameter is promoted to a time-dependent field. Since standard textbooks do not mention representations of such radial fields that are set up on a discretized time mesh from the beginning, the key steps are presented below, following Ref. [31]. In this scheme the partition function takes a form analogous to Eqs. (4-5). However the projection operator does not mix the N time steps and may be written as

$$\begin{aligned} P &= \lim_{N\to\infty}\lim_{W\to\infty}\prod_{n=1}^{N} P_n\,, \quad \text{with} \\ P_n &= \int_{-\infty}^{\infty}\frac{\beta}{N}\frac{d\lambda_n}{2\pi}\int_{-\infty}^{\infty} dx_n\, \mathrm{e}^{-\frac{\beta}{N}(i\lambda_n(x_n-1)+Wx_n(x_n-1))}\,. \end{aligned} \tag{23}$$

Here the constraint parameter λ_n is defined for each time step n, i.e., it is a time-dependent field, and x_n represents the radial slave-boson field at time step n. In the discrete time-step form, the fermionic part of the action reads

$$\begin{aligned} S_f &= \sum_{n=1}^{N}\left\{\sum_{\vec{k}\sigma} c^{\dagger}_{\vec{k},n,\sigma}\left(c_{\vec{k},n,\sigma} - \mathrm{e}^{-\frac{\beta}{N}(\varepsilon_{\vec{k}}-\mu)}\, c_{\vec{k},n-1,\sigma}\right) + \sum_{\sigma} f^{\dagger}_{n,\sigma}\left(f_{n,\sigma} - \mathrm{e}^{-\frac{\beta}{N}(\varepsilon_f+i\lambda_n-\mu)}\, f_{n-1,\sigma}\right)\right\} \\ &+ \frac{\beta}{N}\sum_{n=1}^{N}\sum_{\vec{k}\sigma} V x_n\left(c^{\dagger}_{\vec{k},n,\sigma} f_{n-1,\sigma} + f^{\dagger}_{n,\sigma} c_{\vec{k},n-1,\sigma}\right). \end{aligned} \tag{24}$$

The integration over the fermionic fields can be manifestly carried out. This allows one to obtain the partition function by projecting the resulting fermionic determinant:

$$Z = P\prod_{\sigma}\det\left[S_\sigma\left[\{x_n\},\{\lambda_n\}\right]\right] \tag{25}$$

with the above projection operator Eq. (23). The expectation value of the hole density operator takes the simple form:

$$\langle n_h(\tau_m)\rangle = \langle x_m\rangle = \frac{1}{Z}\,P\left\{x_m\prod_{\sigma}\det\left[S_\sigma\left[\{x_n\},\{\lambda_n\}\right]\right]\right\}\,. \tag{26}$$

It is easily seen to be time-independent. In contrast to a Bose condensate, $\langle x_m\rangle$ is generally finite and may only vanish for zero hole concentration [21]. It is not related to a broken symmetry. The radial slave-boson field exhibits another specific feature: For any power $a > 0$, one finds $\langle x_m^a\rangle = \langle x_m\rangle$, as the corresponding projections of the fermionic determinant all yield the same value.

As concerns the hole autocorrelation function, it is conveniently expressed as a projection of the fermionic determinant. It reads

$$\langle n_h(\tau_n)n_h(\tau_m)\rangle = \langle x_n x_m\rangle = \frac{1}{Z}\,P\left\{x_n x_m\prod_{\sigma}\det\left[S_\sigma\left[\{x_n\},\{\lambda_n\}\right]\right]\right\}. \tag{27}$$

Hence it can be obtained without first determining a self-energy.

Regarding the Kotliar and Ruckenstein representation, it took a long discussion to determine the gauge symmetry group [34–37, 16]. It was finally agreed that it reads $U(1) \times U(1) \times U(1)$. In fact, it could be shown that one may gauge away the phase of three bosonic fields by promoting all three constraint parameters to fields. The fourth one, for example d, remains complex. Therefore, in the $U \to \infty$ limit ($d \to 0$), all three remaining bosonic fields are radial slave-boson fields. In functional integral language they may be handled in the same fashion as the above x-field. For an example, see [22].

4 Saddle-point approximations

The exact evaluation of a quantity represented by a functional integral is an ambitious task. So far, the results are limited to a very small cluster [21, 22] or to the Ising chain [31]. Hence we rather focus on an economical way to determine observable quantities in the SB framework. It is provided by a saddle-point approximation (SPA) to the functional integral and often yields physically reasonable results. This is equivalent to allowing for a finite expectation value of a Bose field amplitude. Strictly speaking, a finite expectation value of a Bose field operator violates gauge invariance and should not exist. In contrast, a finite saddle-point amplitude of the radial slave-boson fields is compatible with Elitzur's theorem. Besides, the saddle-point approximation is exact in the large-degeneracy limit, and the Gaussian fluctuations provide the $1/N$ corrections [16]. Moreover it obeys a variational principle in the limit of large spatial dimensions where the Gutzwiller approximation becomes exact for the Gutzwiller wave function [38]. Furthermore, it could be shown in this limit that longer-ranged interactions are not dynamical and reduce to their Hartree approximation [39]. Therefore, this approach also obeys a variational principle in this limit when applied to the extended Hubbard model Eq. (74).

4.1 Saddle-point approximation to the Barnes representation

In its simplest form, the SPA consists of replacing the boson field operators e_i at each lattice site, or e at the impurity site, by the modulus of its expectation value, in accordance with the above. This yields a non-interacting model, which is easily solved. Below we briefly discuss the solutions for the Anderson impurity model and the Anderson lattice model.

4.1.1 Kondo effect in the Anderson impurity model

In SPA the Anderson impurity Hamiltonian Eq. (1) takes for $U \to \infty$ the form

$$H = \sum_{\vec{k}\sigma} \varepsilon_{\vec{k}}\, c^\dagger_{\vec{k}\sigma} c_{\vec{k}\sigma} + \varepsilon_f \sum_\sigma f^\dagger_\sigma f_\sigma + V \sum_{\vec{k}\sigma} e_0 \left(c^\dagger_{\vec{k}\sigma} f_\sigma + f^\dagger_\sigma c_{\vec{k}\sigma} \right) + \lambda(Q-1)\,. \tag{28}$$

The conserved charge is $Q = \sum_\sigma f^\dagger_\sigma f_\sigma + e_0^2 = 1$, and λ is the corresponding Lagrange multiplier. One recognizes that Eq. (28) describes a resonant-level model with renormalized parameters. They are $\widetilde{\varepsilon}_f = \varepsilon_f + \lambda$ and $\widetilde{V} = V e_0$. Introducing $\widetilde{\Delta} = e_0^2 \Delta = \pi N_F^{(0)} \widetilde{V}^{\,2}$, where $\Delta = \pi N_F^{(0)} V^2$

($N_F^{(0)} = 1/2D$ is the conduction electron DOS at the Fermi level) allows one to write the saddle-point equations in the form of two conditions for the level position $\widetilde{\varepsilon}_f$ and the level width $\widetilde{\Delta}$. They are

$$\widetilde{\varepsilon}_f = \varepsilon_f - \frac{2\Delta}{\pi} \ln \frac{\sqrt{\widetilde{\varepsilon}_f^2 + \widetilde{\Delta}^2}}{D} \text{ and } \quad \widetilde{\Delta} = \Delta - \frac{2\Delta}{\pi} \tan^{-1} \frac{\widetilde{\Delta}}{\widetilde{\varepsilon}_f} \,. \tag{29}$$

In the limit of $\Delta \ll |\varepsilon_f|$, the occupation of the local level $n_f = \frac{2/\pi}{\tan}^{-1} \frac{\widetilde{\Delta}}{\widetilde{\varepsilon}_f}$ approaches unity. This means that a local moment forms at higher temperature. Below a characteristic temperature, the Kondo temperature T_K, the local moment gets screened by the conduction electron spins, which form a resonance state with the local moment. It is located close to the Fermi energy, at $\widetilde{\varepsilon}_f$, and is of width $\widetilde{\Delta} \approx T_K = D \exp \frac{-|\varepsilon_f|}{2N_F^{(0)} V^2} = D \exp \frac{-1}{2N_F^{(0)} J}$, where $J = \frac{V^2}{|\varepsilon_f|}$ is the antiferromagnetic spin exchange coupling constant of the local spin and the local conduction electron spin density. The low-temperature behavior of Kondo systems is reasonably well described by SB mean-field theory. Yet at higher temperatures, a spurious first-order transition to the local-moment regime is found in this approximation rather than a continuous crossover.

As an alternative scheme, Kroha *et al.* [40] developed an approximation that guarantees local gauge invariance in a conserving approximation and allows for Fermi-liquid as well as non-Fermi liquid behavior for the investigated multi-channel Anderson impurity problem.

4.1.2 Heavy fermions in the Anderson lattice model

The Anderson lattice model in the limit $U \to \infty$ has been investigated in the SB mean-field approximation [33], in which the Hamiltonian reads again as a single-particle Hamiltonian, but for two hybridized bands

$$H = \sum_{\vec{k}\sigma} \varepsilon_{\vec{k}}\, c^\dagger_{\vec{k}\sigma} c_{\vec{k}\sigma} + \varepsilon_f \sum_{i,\sigma} f^\dagger_{i\sigma} f_{i\sigma} + V \sum_{i,\sigma} e_0 \left(c^\dagger_{i\sigma} f_{i\sigma} + f^\dagger_{i\sigma} c_{i\sigma} \right) + \sum_i \lambda_i (Q_i - 1) \,. \tag{30}$$

The saddle-point condition with respect to the field λ_i leads to the condition $\langle Q_i \rangle = 1$. For a translationally invariant state it is independent of the lattice position $\vec{R}_i$. As in the impurity problem, the f-level position is shifted by correlation effects to $\tilde{\varepsilon}_f$, and the square of the boson amplitude is related to the f-level occupation n_f through:

$$\widetilde{\varepsilon}_f \;=\; \varepsilon_f - 2N_F^{(0)} V^2 \ln \frac{\widetilde{\varepsilon}_f - \varepsilon_F}{D} \tag{31}$$

$$e_0^2 \;=\; 1 - n_f = 1 - \frac{2N_F^{(0)} V^2 e_0^2}{\widetilde{\varepsilon}_f} \,, \tag{32}$$

under the assumption $|\widetilde{\varepsilon}_f| \ll D$. In the case where ε_f is sufficiently below the Fermi level ε_F we have $|\widetilde{\varepsilon}_f| \ll |\varepsilon_f|$ and, from Eq. (31), we observe that $\widetilde{\varepsilon}_f - \varepsilon_F = D \exp \frac{-|\varepsilon_f|}{2N_F^{(0)} V^2} = T_K$, equal to the single-impurity Kondo temperature. In this limit $e_0^2 \approx |\widetilde{\varepsilon}_f| / 2N_F^{(0)} V^2 \ll 1$. Thus, the hybridization amplitude is substantially reduced, leading to heavy quasiparticle bands of energy

$$E^\pm_{\vec{k}} = \frac{1}{2} \left[\varepsilon_{\vec{k}} + \widetilde{\varepsilon}_f \pm \sqrt{(\varepsilon_{\vec{k}} + \widetilde{\varepsilon}_f)^2 + V^2 e_0^2} \right] \,. \tag{33}$$

4.2 Saddle-point approximation to the Kotliar and Ruckenstein representation

Extending this approach to the Hubbard Model on the lattice has also been achieved. Yet at this stage of the formulation, the representation suffers from the drawback that neither the low-charge-carrier-density limit nor the non-interacting limit are properly recovered on the SPA level [14], in contrast to more conventional approaches. Kotliar and Ruckenstein overcame this difficulty by noticing that there is no unique SB representation but rather infinitely many different ones. If faithful, they are all equivalent when the functional integral is exactly evaluated but differ on the saddle-point level. Kotliar and Ruckenstein provided us with a representation of the kinetic energy that solves both aspects of the above drawback. The KR representation consists of replacing the operators $\tilde{z}_\sigma$ in Eq. (9) by

$$z_\sigma = e^\dagger L_\sigma R_\sigma p_\sigma + p^\dagger_{-\sigma} L_\sigma R_\sigma d \text{ , with} \tag{34}$$

$$L_\sigma = \frac{1}{\sqrt{1 - p^\dagger_\sigma p_\sigma - d^\dagger d}} \quad \text{and} \quad R_\sigma = \frac{1}{\sqrt{1 - p^\dagger_{-\sigma} p_{-\sigma} - e^\dagger e}} \tag{35}$$

and of consistently using $a_\sigma = z_\sigma f_\sigma$ in the representation of the kinetic energy operator. In this form, the SPA to the KR representation is equivalent to the Gutzwiller approximation (GA) to the Gutzwiller wave function [14]. As the GA yields the exact energy of the Gutzwiller wave function in the large-dimensionality limit, the SPA to the KR representation acquires a variational principle in this limit. In addition it turns exact in several large N limits [16], or for particular toy models [41]. These properties are shared by the SRI formulation [16]. Indeed, introducing $\tilde{p}_{\sigma\sigma'} \equiv \sigma\sigma' p_{-\sigma',-\sigma}$, the z operator reads

$$\underline{z} = e^\dagger \underline{L}\ M\ \underline{R}\ \underline{p}\ + \underline{\tilde{p}}^\dagger \underline{L}\ M\ \underline{R}\ d \tag{36}$$

with

$$M = \left[1 + e^\dagger e + \sum_\mu p^\dagger_\mu p_\mu + d^\dagger d \right]^{\frac{1}{2}} \quad , \tag{37}$$

$$\underline{L}\ = \left[\left(1 - d^\dagger d\right) \underline{1} - 2\underline{p}^\dagger \underline{p}\ \right]^{-\frac{1}{2}} \quad \text{and} \quad \underline{R} = \left[\left(1 - e^\dagger e\right) \underline{1} - 2\underline{\tilde{p}}^\dagger \underline{\tilde{p}}\ \right]^{-\frac{1}{2}} \ . \tag{38}$$

Eq. (36) and Eq. (38) correct Eq. (22) in [16] and Eq. (38) corrects Eq. (3) in [42].

4.2.1 Mott-Hubbard metal-to-insulator transition

The KR and SRI representations have been used to characterize a broad range of phases of the Hubbard Model [43–57], as they are able to capture interaction effects beyond the physics of a Slater determinant. These representation encompass the Brinkman-Rice mechanism [58, 59], described below, allowing for the description of the Mott metal-to-insulator transition. This transition is a genuine interaction-driven transition that is not linked to a period doubling resulting from, e.g., an antiferromagnetic instability. On the contrary, it arises when considering the paramagnetic saddle point. In the SRI representation, it corresponds to setting the bosonic

fields $\vec{p}_i(\tau)$ and the constraint fields enforcing Eq. (15) to zero and to replacing the remaining bosonic and constraint fields by their mean value. The free energy then reads

$$F = -T \sum_{\vec{k},\sigma} \ln\left(1 + \mathrm{e}^{-\frac{E_{\vec{k}\sigma}}{T}}\right) + U\, d^2 + \alpha\left(e^2 + p_0^2 + d^2 - 1\right) - \beta_0\left(p_0^2 + 2d^2\right). \tag{39}$$

Here the Lagrange multiplier α (β_0) enforces the constraints of Eq. (13) and (14). With

$$z_0 = \frac{1}{\sqrt{2}} \frac{p_0(e+d)}{\sqrt{1 - d^2 - \frac{1}{2}p_0^2}\,\sqrt{1 - e^2 - \frac{1}{2}p_0^2}} \tag{40}$$

the quasiparticle dispersion relation is given by

$$E_{\vec{k}\sigma} = z_0^2\, t_{\vec{k}} + \beta_0 - \mu\,. \tag{41}$$

z_0^2 plays the role of both a mass renormalization factor and of a quasiparticle residue. In the parameter range in which it vanishes, a Mott insulating state is realized. Solving the saddle-point equations at half filling $\rho = 1$ yields

$$z_0^2 = 1 - \left(\frac{U}{U_c}\right)^2 \text{, with} \quad U_c = -4 \sum_{\vec{k},\sigma} t_{\vec{k}}\, f_F(z_0^2\, t_{\vec{k}})\,, \tag{42}$$

where f_F is the Fermi function. Therefore, the quasiparticle residue continuously varies from 1 down to 0 for $U \to U_c$. At this point, the quasiparticle mass diverges and its residue vanishes, signaling a metal-to-insulator transition. As an additional signature of a transition, a Mott gap opens. Indeed, solving the equation for the chemical potential of the quasiparticles for $U > U_c$ and $\rho \to 1$ yields [35]

$$\mu(\rho) = \frac{U}{2}\left[1 - \frac{1-\rho}{|1-\rho|}\sqrt{1 - \frac{U_c}{U}}\right]. \tag{43}$$

The discontinuity in μ across $\rho = 1$ indicates a pair of first-order phase transitions from the metallic phase at $\rho < 1$ (with finite z_0) to the insulating phase at $\rho = 1$ (with chemical potential $\mu = U/2$) and back to the metallic phase at $\rho > 1$ (with finite z_0). This discontinuity vanishes for $U \to U_c^+$, which is therefore a critical point. In the insulating phase the quasiparticle contribution to doubly occupied sites vanishes. This does not imply that the latter is predicted to be zero but that it purely results from fluctuations, which we address in Sec. 5.
The saddle-point equations following from the free energy Eq. (39) read

$$\begin{aligned}
p_0^2 + e^2 + d^2 - 1 &= \quad 0\,, \\
p_0^2 + 2d^2 &= \quad \rho\,, \\
\frac{1}{2e}\frac{\partial z_0^2}{\partial e}\,\bar{\varepsilon} &= -\alpha\,, \\
\frac{1}{2p_0}\frac{\partial z_0^2}{\partial p_0}\,\bar{\varepsilon} &= \quad \beta_0 - \alpha\,, \\
\frac{1}{2d}\frac{\partial z_0^2}{\partial d}\,\bar{\varepsilon} &= \quad 2(\beta_0 - \alpha) + \alpha - U.
\end{aligned} \tag{44}$$

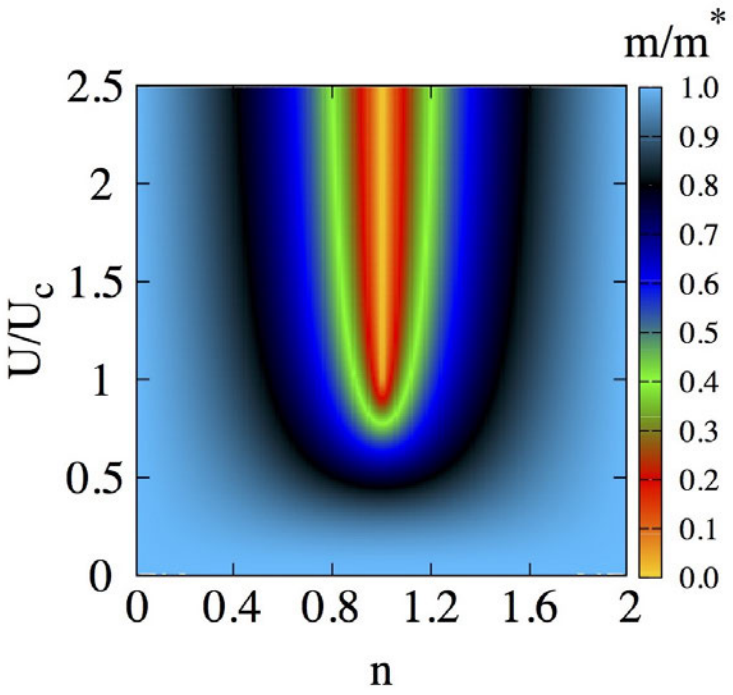

Fig. 1: *Inverse effective mass z_0^2 for the Hubbard model on the cubic lattice.*

Here we have introduced the averaged kinetic energy,

$$\bar{\varepsilon} = \int d\omega\, \rho(\omega)\, \omega\, f_F\big(z_0^2\, \omega + \beta_0 - \mu\big)\,, \tag{45}$$

the determination of which involves the density of states $\rho(\omega)$. Introducing the doping away from half filling $\delta = 1 - \rho$, the Coulomb parameter $u = U/(-8\bar{\varepsilon})$, and $y \equiv (e+d)^2$, the saddle-point equations can be cast into a single one that finally reads

$$y^3 + (u-1)y^2 = u\,\delta^2. \tag{46}$$

For more details see Ref. [16, 59]. In the case of a 3D cubic lattice the quasiparticle mass diverges at half filling for $U_c \simeq 16.04\,t$. This behavior is general, and the transition occurs for other lattices in a qualitatively equivalent way. For instance, in the case of a 2D square lattice, the metal-to-insulator transition occurs at $U_c = 2(8/\pi)^2 t$. Note that the ratio of the critical interaction for the 3D cubic lattice to the one of the 2D square lattice (1.24) is somewhat smaller that the naive estimate that would be obtained from the corresponding ratio of the number of nearest neighbors (3/2). In the case of a rectangular DOS one has $U_c = W$.

Regarding the doping dependence of the quasiparticle residue, Fig. 1 shows that a mass renormalization larger than 2 is only realized in the regime of large $U > \frac{3}{4}U_c$ and doping $|\delta| < 0.25$. In the limits $U \to 0$ and $|\delta| \to 1$, the saddle-point approximation correctly yields the exact result $z_0^2 = 1$. Further, calculations performed for the 2D square lattice yield a figure very similar to Fig. 1.

4.3 Saddle-point approximation to the multi-band Hubbard model

We now turn to the multi-band Hubbard model that is often used for the description of transition-metal oxides. As in the case of the one-band Hubbard model, the non-interacting limit is not properly recovered when representing the electron operator a_α according to Eq. (18) as $\tilde{z}_\alpha f_\alpha$ in the kinetic energy term. This difficulty may be overcome in a fashion analogous to the one followed in the framework of the Kotliar and Ruckenstein representation to the one-band Hubbard model: One represents the electron operator a_α as $z_\alpha f_\alpha$ where

$$z_\alpha = \sum_{m=1}^{2M} \sum_{\alpha_1<\cdots<\alpha_{m-1}} \psi^{(m)}_{\alpha,\alpha_1,\ldots,\alpha_{m-1}} L_\alpha R_\alpha \psi^{\dagger(m-1)}_{\alpha_1,\ldots,\alpha_{m-1}} \tag{47}$$

involves the normalization factors L_α and R_α. They are now given by

$$\begin{aligned} R_\alpha &= \left[1 - \sum_{m=0}^{2M-1} \sum_{\alpha_1,<\cdots<,\alpha_m} \psi^{\dagger(m)}_{\alpha_1,\ldots,\alpha_m} \psi^{(m)}_{\alpha_1,\ldots,\alpha_m}\right]^{-\frac{1}{2}} \qquad \alpha_i \neq \alpha \\ L_\alpha &= \left[1 - \sum_{m=1}^{2M} \sum_{\alpha_1<\cdots<\alpha_{m-1}} \psi^{\dagger(m)}_{\alpha,\alpha_1,\ldots,\alpha_{m-1}} \psi^{(m)}_{\alpha,\alpha_1,\ldots,\alpha_{m-1}}\right]^{-\frac{1}{2}} . \end{aligned} \tag{48}$$

Namely L_α normalizes to 1 the probability that no electron in state $|\alpha\rangle$ is present on a site before one such electron hops to that particular site, and R_α makes sure that it happened. Clearly the eigenvalues of the operators L_α and R_α are 1 in the physical subspace.

We now proceed to the saddle-point approximation, and we investigate the Mott transition at commensurate integer filling n for an M-band model. In order to highlight general features of the model, we first consider the paramagnetic, paraorbital phase at $J_H = 0$. The latter is obtained after having integrated out the fermions, setting all bosonic fields to their averaged value, and, for given m, demanding that the various $\psi^{(m)}_{\alpha_1<\cdots<\alpha_m}$ are equal to one another. The Mott transition that occurs at commensurate density n is most conveniently discussed by projecting out occupancies that are larger than $n+1$ and smaller than $n-1$ (if any), as they would at most play a subleading role. The constraint allows for eliminating the variables $\psi^{(n-1)}$ and $\psi^{(n)}$ obtaining the free energy at filling n as

$$F(D) = (1-2D^2)\, D^2 \left(\sqrt{b_{n,M}} + \sqrt{c_n}\right)^2 \bar{\varepsilon} + U\left(D^2 + \binom{n}{2}\right), \tag{49}$$

with $\bar{\varepsilon} \equiv \int d\epsilon\, \epsilon\, \rho(\epsilon)\, f_F(z^2\epsilon + \lambda_0 - \mu)$, $D^2 \equiv \binom{2M}{n+1} \psi^{(n+1)2}$, $b_{n,M} \equiv (2M-n+1)/(2M-n)$, and $c_n \equiv (n+1)/n$. Here, $\rho(\epsilon)$ is the total DOS. Minimizing Eq. (49) with respect to D yields a critical interaction strength at which D vanishes. It depends on n and M and reads

$$U_c^{(n,M)} = -\bar{\varepsilon}\left(\sqrt{b_{n,M}} + \sqrt{c_n}\right)^2, \tag{50}$$

which reproduces the results of the Gutzwiller approximation [13, 76]. This locates the Mott transition. In the often considered case of a rectangular DOS, the critical interaction strength may be related to the band width W through

$$U_c^{(n,M)} = \frac{nW}{4M}(2M-n)\left(\sqrt{b_{n,M}} + \sqrt{c_n}\right)^2. \tag{51}$$

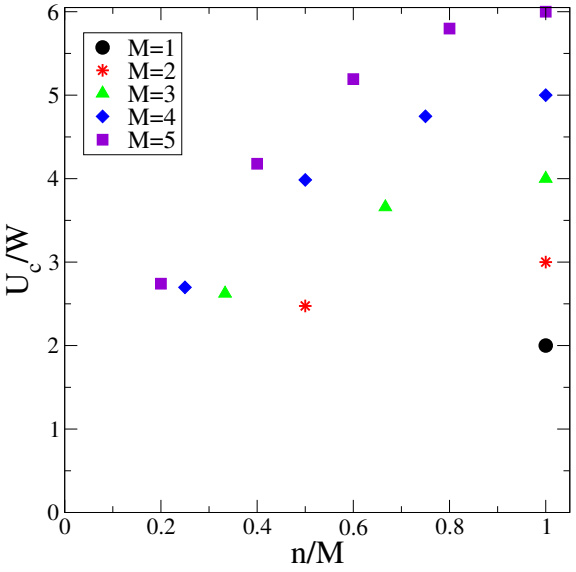

Fig. 2: *Dependence of the location of the Mott transition on the filling n and the band degeneracy M for the particle-hole symmetric rectangular density of states.*

As shown in Fig. 2, it weakly depends on the band degeneracy for fixed filling n, but quite significantly on n for a given band degeneracy.
The effective mass of the quasiparticles diverges when reaching the Mott point. We obtain the analytical behavior as

$$\frac{m}{m^*} = z_0^2 = \frac{\left(\sqrt{b_{n,M}} + \sqrt{c_n}\right)^2}{8} \quad \frac{U_c^{(n,M)2} - U^2}{U_c^{(n,M)2}}. \tag{52}$$

The dependence on the band degeneracy is weak as a consequence of the particular form of the coefficients $b_{n,M}$ and c_n. As the critical interaction strength increases with M the quasiparticle residue $Z = z_0^2$ increases slightly with M. However, for small values of U and without projecting out higher occupancies, Z actually decreases with increasing M. There is therefore a crossover value of the interaction strength beyond which the system becomes more metallic with increasing M [17].
As a function of the hole doping δ, the quasi particle residue vanishes for δ going to 0 above $U_c^{(n,M)}$ as

$$z_0^2 = \frac{\delta}{2}\left(b_{n,M} - c_n\right) + \frac{|\delta|}{2}\left(\left(b_{n,M} + c_n\right)\sqrt{1 + 4\varphi_{n,M}} + 4\sqrt{b_{n,M} c_n \varphi_{n,M}}\right) \tag{53}$$

where we introduced:

$$\varphi_{n,M} \equiv \frac{U_c^{(n,M)^2} \dfrac{b_{n,M} c_n}{\left(\sqrt{b_{n,M}} + \sqrt{c_n}\right)^4}}{\left(U - U_c^{(n,M)}\right)\left(U - U_c^{(n,M)}\left(\dfrac{\sqrt{b_{n,M}} - \sqrt{c_n}}{\sqrt{b_{n,M}} + \sqrt{c_n}}\right)^2\right)}. \tag{54}$$

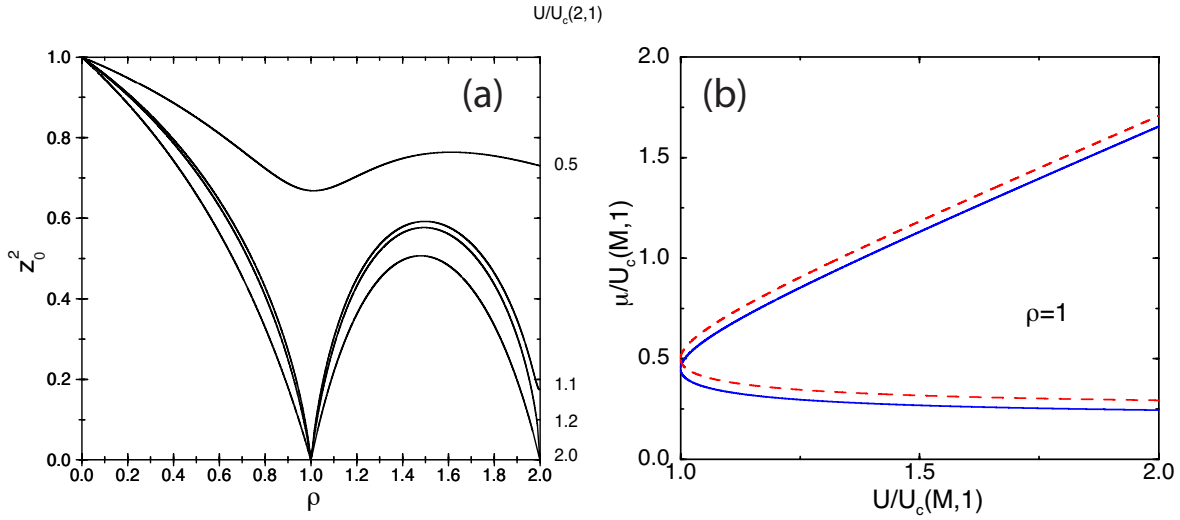

Fig. 3: *(a) Inverse effective mass in the two-band model as a function of density for several values of U. (b) Chemical potential for $n = 1$ for the one-band (dashed line) and two-band (full line) models.*

This expression of the quasiparticle residue consists of two contributions that are either symmetric or antisymmetric with respect to particle or hole doping. The particle-hole symmetry requires the antisymmetric contribution to vanish for $n = M$. We observe that the asymmetry of z_0^2 on particle or hole doping increases under an increase of $|n - M|$. It vanishes more slowly for hole doping (for $n \leq M$) than for particle doping, for increasing degeneracy at fixed n, for increasing degeneracy at $n = M$, and under an increase of U. As an example, we calculate the effective mass for the two-band model, which has been calculated without projecting out higher occupancies, and show it in Fig. 3a.

Analogously to the one-band case we obtain a Mott gap. Indeed, the number of quasiparticles is a continuous function of their chemical potential $\mu - \lambda_0/2$. The constraint parameters Λ and λ as well as μ jump when going through the Mott gap. The Mott gap $\Delta \equiv \lim_{\delta\to 0^-} \mu(\delta) - \lim_{\delta\to 0^+} \mu(\delta)$ results as

$$\Delta = \sqrt{(U - U_c^{(n,M)}) \left(U - U_c^{(n,M)} \left(\frac{\sqrt{b_{n,M}} - \sqrt{c_n}}{\sqrt{b_{n,M}} + \sqrt{c_n}} \right)^2 \right)}. \tag{55}$$

In the limiting case of $U \gg U_c^{(n,M)}$, the Mott gap is given by U, while it closes at $U_c^{(n,M)}$ as $\Delta \sim U_c^{(n,M)} \sqrt{U/U_c^{(n,M)} - 1}$, the square root behavior being typical of slave-boson mean-field theories. It is displayed in Fig. 3b, where it is compared to the one-band case as obtained by Lavagna [35]. Clearly, no big difference in the Mott gap is found when going from one band to two bands. In fact $\Delta/U_c^{(n,M)}$ is independent of M at $n = M$, while for fixed n the dependence on M is very weak. For a comparison to the experimental situation in the titanates see Ref. [17].

4.3.1 Influence of Hund's rule coupling

The Hund's rule coupling turns out to have a deep influence on the nature of the Mott transition. As an example we treat here the two-band model around the $n = 1$ Mott insulating lobe. At density $\rho = 1$ we obtain the saddle-point free energy as

$$F = \frac{4}{3}\bar{\varepsilon}\left(1-2r^2\right)\left(r + (d_0 + d_x + \Delta_0)/\sqrt{2}\right)^2 + (U+3J)\,\Delta_0^2 + (U+J)\,d_x^2 + U\,d_0^2. \quad (56)$$

with $\bar{\varepsilon} \equiv \int d\epsilon\,\epsilon\,\rho(\epsilon)\,f_F(z^2\epsilon + \lambda_0 - \mu)$, $d_0 \equiv (\psi^{(2)}_{\uparrow,\uparrow} + \psi^{(2)}_{\downarrow,\downarrow})/\sqrt{2}$, $d_x \equiv (\psi^{(2)}_{\uparrow,\downarrow} + \psi^{(2)}_{\downarrow,\uparrow})/\sqrt{2}$, $\Delta_0 \equiv (\psi^{(2)}_{\uparrow\downarrow,0} + \psi^{(2)}_{0,\downarrow\uparrow})/\sqrt{2}$, $r^2 \equiv d_0^2 + d_x^2 + \Delta_0^2$, and $\lambda \equiv \sum_\alpha \lambda_\alpha/2$, and we have used the constraints to remove the variables $\psi^{(0)}$ and $\psi^{(1)}$. Let us notice that this expression differs from an ordinary Ginzburg-Landau free energy in that it cannot be written as a fourth-order polynomial in the variables d_0, d_x, and Δ_0. Therefore, a critical point for one field would be critical for the other ones as well. Lacking an analytical expression for the location of the Mott transition for arbitrary J_H/U, we first focus on the small J_H/U regime. We find

$$U_c^{(1,2)}(J_H) = U_c^{(1,2)}(0)\left(1 - \frac{4}{3}\quad\frac{J_H}{U} + \mathcal{O}(J_H/U)^2\right). \quad (57)$$

Hence $U_c^{(1,2)}$ first decreases linearly with J_H. Another regime of interest is the large J_H regime. There we obtain the location of the Mott transition as

$$U_c^{(1,2)} = -\frac{2}{3}\bar{\varepsilon}\,(3+2\sqrt{2})\left(1 - \frac{8}{9}\frac{\bar{\varepsilon}}{J_H}\right) + \mathcal{O}\left(\frac{\bar{\varepsilon}}{J_H}\right)^2 \quad (58)$$

and thus decreasing J from ∞ leads to an increase of the critical interaction. Another intriguing feature of transition-metal oxides such as V_2O_3 is the metal-to-insulator transition that occurs in the vicinity of the tri-critical point under an increase of temperature. It has been interpreted [60] as the transition from a Fermi liquid with finite quasiparticle residue Z to an insulator with $Z = 0$. In other words, there is a finite coherence temperature T_{coh} at which the coherence of the Fermi liquid (and Z) vanishes. This result was obtained in the dynamical mean-field approximation to the one-band model, which becomes exact in the limit of large dimensions and is recovered in the Gutzwiller approximation [61]. At finite T there is a first-order metal-to-insulator transition at a critical $U_c^{(1,M)}(T)$

$$U_c^{(1,M)}(T) = U_c^{(1,M)}(0) - \sqrt{8U_c^{(1,M)}(0)\,T\ln 2M}\,. \quad (59)$$

Thus an increase in temperature may produce a metal-to-insulator transition, which is consistent with the experimental situation in V_2O_3. In the dynamical mean-field approximation at finite temperatures there is an interaction strength $U_{c2}(T)$ at which the metallic solution ceases to exist. This quantity can also be evaluated in this SB scheme and is given by

$$U_{c2}^{(1,M)}(T) = U_c^{(1,M)}(0)\left(1 - \alpha_M (T/W)^{\frac{2}{3}}\right), \quad (60)$$

with $\alpha_1 \sim 2.53$ for the one-band model, and $\alpha_2 \sim 3.32$ for the two-band model.

4.4 A concrete example

We now proceed with an example that builds on a model for the anisotropic superconductor Sr_2RuO_4. This two-band model includes a finite J_H and an effective kinetic energy term that derives from a tight-binding Hamiltonian. As suggested by Noce and Cuoco [62], the bands crossing the Fermi energy build on the Ru $4d$ d_{xz}- and d_{yz}-orbitals as well as on the O $2p_z$-orbitals. Following Ref. [63], we integrate out the latter. This yields the effective model

$$H_0 = \sum_{\vec{k},\sigma} \left(d^\dagger_{xz,\vec{k},\sigma},\ d^\dagger_{yz,\vec{k},\sigma} \right) \begin{pmatrix} e_{\vec{k}} & a_{\vec{k}} \\ a_{\vec{k}} & f_{\vec{k}} \end{pmatrix} \begin{pmatrix} d_{xz,\vec{k},\sigma} \\ d_{yz,\vec{k},\sigma} \end{pmatrix}, \tag{61}$$

with $a_{\vec{k}} = -4\,t' \sin k_x \sin k_y$, $e_{\vec{k}} = t \cos k_x$, and $f_{\vec{k}} = t \cos k_y$. The two pairs of bands $E_{\vec{k},\nu,\sigma}$ with

$$E_{\vec{k},\nu,\sigma} = \frac{1}{2}\left(e_{\vec{k}} + f_{\vec{k}}\right) + \frac{1}{2}\,\nu\,\sqrt{\left(e_{\vec{k}} - f_{\vec{k}}\right)^2 + 4a^2_{\vec{k}}}, \quad \nu = \pm 1 \tag{62}$$

acquire two-dimensional character because of the finite t'.
On the slave-boson SPA level the free energy reads

$$\begin{aligned} F &= -\frac{1}{\beta}\sum_{\vec{k},\nu,\sigma} \ln\left(1 + e^{-\beta E_{\vec{k},\nu,\sigma}}\right) + U \sum_i \left(\sum_{\alpha<\alpha'} d^2_{i,\alpha\alpha'} + 3 \sum_{\alpha<\alpha'<\alpha''} t^2_{i,\alpha\alpha'\alpha''} + 6q_i^2 \right) \\ &+ J_H \sum_i \left(\sum_\sigma d^2_{i,xz\sigma,yz-\sigma} + 3\sum_\rho d^2_{i,\rho\uparrow,\rho\downarrow} + 4 \sum_{\alpha<\alpha'<\alpha''} t^2_{i,\alpha\alpha'\alpha''} + 8q_i^2 \right) \\ &+ \sum_i \Lambda_i \left(e_i^2 + \sum_\alpha p^2_{i\alpha} + \sum_{\alpha<\alpha'} d^2_{i,\alpha\alpha'} + \sum_{\alpha<\alpha'<\alpha''} t^2_{i,\alpha\alpha'\alpha''} + q_i^2 - 1 \right) \\ &- \sum_{i,\alpha} \beta_{i,\alpha} \left(p^2_{i,\alpha} + \sum_{\alpha'} d^2_{i,\alpha\alpha'} + \sum_{\alpha'\alpha''} t^2_{i,\alpha\alpha'\alpha''} + q_i^2 \right) \end{aligned} \tag{63}$$

Here the bosons e, p_α, $d_{\alpha\alpha'}$, $t_{\alpha\alpha'\alpha''}$, and q refer to occupancies zero, one, two, three, and four, respectively. The Lagrange multipliers Λ and β_α enforce the constraints Eq. (20) and Eq. (21), respectively. In a paramagnetic or a ferromagnetic phase, the dispersions of the quasiparticles are given by

$$E_{k,\nu,\sigma} = \frac{1}{2}\left[\beta_{xz,\sigma} + \beta_{yz,\sigma} - 2\mu + \left(z^2_{xz,\sigma}\tilde{e}_k + z^2_{yz,\sigma}\tilde{f}_k \right) + \nu \sqrt{\left(z^2_{xz,\sigma}\tilde{e}_k - z^2_{yz,\sigma}\tilde{f}_k \right)^2 + 4 z^2_{xz,\sigma} z^2_{yz,\sigma} \tilde{a}^2_k} \right] \tag{64}$$

where the dependence on σ is effective in the ferromagnetic phase only. The mass renormalization factors are constructed according to Eq. (47).

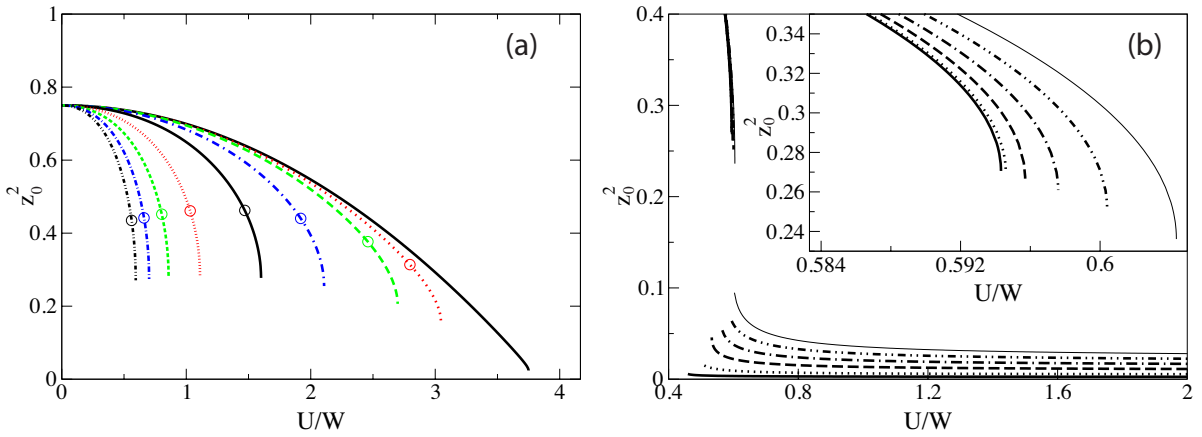

Fig. 4: *(a) Effective mass renormalization at $\rho = 2$ for J_H/U= 0 (thick full line), 0.01 (thick dotted line), 0.02 (thick dashed line), 0.05 (thick dashed-dotted line), 0.1 (thin full line), 0.2 (thin dotted line), 0.3 (thin dashed line), 0.4 (thin dashed-dotted line) and 0.5 (thin dashed-dotted-dotted line). The circles indicate the location of the first order transition. (b) Effective mass renormalization off half filling for J_H/U= 0.5 and $\rho = 2.005$ (full line), 2.01 (dotted line), 2.02 (dashed line), 2.03 (dashed-dotted line), 2.04 (dashed-dotted-dotted line), and 2.05 (thin full line). Inset: Blow-up of the metallic solutions with the same parameters.*

The saddle-point equations have been solved on a 800×800 lattice, at a temperature $T = t/1000$. We neglected four-fold occupancies and empty configurations since the electronic density in the ruthenates under study is $\rho \sim 2$. This approximation is justified in the vicinity of the Mott transition but breaks down for densities above three (below one) and for weak coupling, where our results should be taken with care. It is now well established that the Hund's rule coupling has a strong influence on the Mott transition. While the latter is second-order for $J_H = 0$ and $\rho = 2$ or for any J_H for $\rho = 1$ or 3, it becomes first-order for finite J_H at half filling as shown in Fig. 4a. In fact, no diverging effective mass is found. Instead, the metallic solution of the saddle-point equations ceases to exist at a critical value U_{c2}. Moreover the effective mass is at most renormalized by a factor of five for $J_H/U \geq 0.01$, in contrast to the one-band case. The saddle-point equations also possess an insulating paramagnetic solution: It is characterized by a vanishing value of all bosons except $d_{xz,\sigma}$ and $d_{yz,\sigma}$ and therefore a diverging effective mass (for finite J_H). It extends down to $U_{c1} = 0$. We remark that U_{c2} is only slightly larger than U_c, where the energy of the metallic and insulating solutions coincide. Consequently, the effective mass renormalization is even more modest in the metallic phase. Finally, Fig. 4a also shows that U_c strongly depends on J_H.

Once the system is doped the situation changes little by little. For small electron doping, the first-order transition remains but gradually vanishes with increasing electron concentration as shown in Fig. 4b. The metallic solution is only modestly affected, except that it allows for decreasing values of z in the vicinity of the Mott transition. The insulating solution becomes metallic under electron doping, and the truly insulating state is only found for integer fillings. However the effective mass renormalization remains very large, and accordingly the quasi particle residue is small. Under these circumstances, magnetic or even striped phases are likely to set in, and in addition the system may well be strongly influenced by other interaction terms,

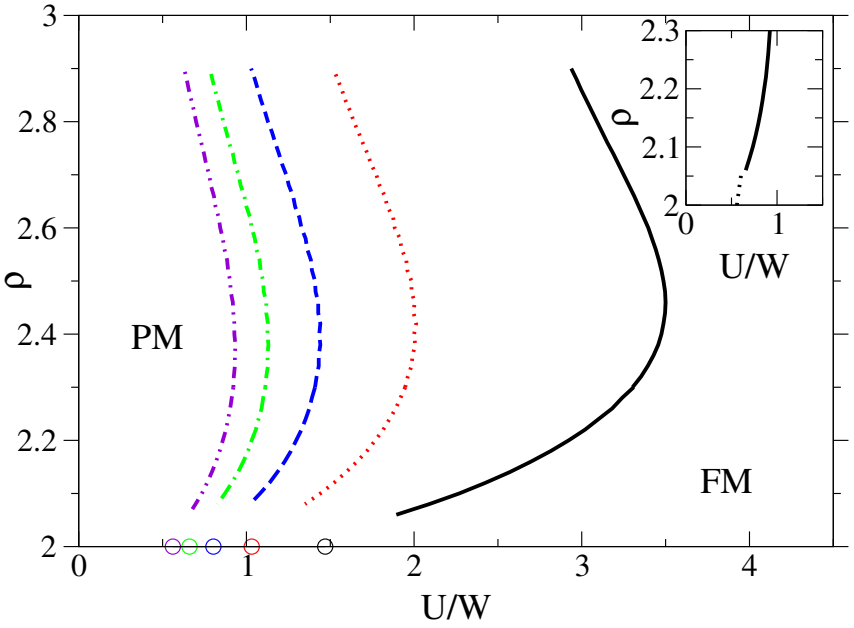

Fig. 5: *Instability line towards ferromagnetism in the ρ-U plane for J_H/U= 0.1 (full line), 0.2 (dotted line), 0.3 (dashed line), 0.4 (dashed-dotted line), and 0.5 (dashed-dotted-dotted line). The circles are indicating the corresponding U_c at half filling. Inset: Instability line (full line), and first-order transition line (dotted line), for J_H/U=0.5.*

as reviewed by Vollhardt *et al.* [64], or disorder effects. This gives a qualitative explanation as to why many transition-metal oxides remain insulating even upon substantial doping, such as $La_{1-x}Ca_xVO_3$ [65] (for a review, see [66]).

The instabilities of the paramagnetic phases towards ferromagnetism are collected in Fig. 5, for several values of J_H/U. For large values of the latter, the range of stability of the paramagnetic phase is seen to depend weakly on density. In contrast, it may extend to large interaction strengths for $J_H/U = 0.1$. On top, there is a strong asymmetry around $\rho = 2.5$, which mostly follows from the difference between $U_c^{(2,2)}$ and $U_c^{(3,2)}$ and not from the neglecting of four-fold occupancies. As displayed in the inset of Fig. 5, the instability lines connect to the first-order transition line separating two paramagnetic solutions, where the latter ends, within numerical accuracy. No ferromagnetic solution, even with very small magnetization, has been found for very small doping and $U > U_c$.

When comparing this phase diagram to La-doped Ca_2RuO_4, we see that a small amount of electron doping turns a Mott insulator into a ferromagnet, in agreement with experiment [67].

It should also be remarked that ferromagnetic instabilities only arise in the doped Mott insulating regime or, in other words, that ferromagnetism is a property of electrons undergoing strong local interactions.

An experimental attempt to reach such a ferromagnetic instability by enhancing the electronic correlations due to the reduction of the bandwidth in two-dimensional superlattices resulted in a ferromagnetic state with a high Curie temperature [30]. Yet the exact underlying effects seem to be more complex than the sole reduction of the dimensionality [68].

4.5 Magnetic order in the Anderson lattice model

The Anderson lattice model is believed to describe the physics of many transition-metal oxides aw well as rare-earth and actinide compounds, including the so-called heavy fermion compounds. It is one of the archetypical models of correlated electrons on a lattice: It consists of a light conduction band hybridized with a strongly correlated narrow f-electron band. The physics is influenced by the strength of the onsite Coulomb repulsion in the f orbital, the hybridization strength, and the band filling. Depending on the values of these parameters, the model describes either localized moments interacting via spin exchange interaction (e.g. the RKKY interaction), which usually order at low temperature, or Kondo screened moments and heavy quasiparticles. The competition between these two ground states gives rise to a quantum phase transition [69, 70]. A qualitatively correct description (excluding the critical behavior at the quantum critical point, which requires a different approach) may be obtained within the SRI slave-boson SPA. The Hamiltonian of the Anderson lattice model reads

$$H = \sum_{\vec{k}\sigma} \varepsilon_{\vec{k}}\, c^\dagger_{\vec{k}\sigma} c_{\vec{k}\sigma} + \varepsilon_a \sum_{i,\sigma} a^\dagger_{i\sigma} a_{i\sigma} + V \sum_{i,\sigma} \left(c^\dagger_{i\sigma} a_{i\sigma} + a^\dagger_{i\sigma} c_{i\sigma} \right) + U \sum_i a^\dagger_{i\uparrow} a_{i\uparrow} a^\dagger_{i\downarrow} a_{i\downarrow}\,, \qquad (65)$$

where $c_{i\sigma} = \sum_{\vec{k}} \mathrm{e}^{i\vec{k}\cdot\vec{R}_i}\, c_{\vec{k}\sigma}$ and $\vec{R}_i$ is the lattice vector at site i. H may be represented in terms of SRI slave-boson operators as

$$\begin{aligned} H = & \sum_{\vec{k}\sigma} \varepsilon_{\vec{k}}\, c^\dagger_{\vec{k}\sigma} c_{\vec{k}\sigma} + \varepsilon_a \sum_i \left(\sum_\mu p^\dagger_{i\mu} p_{i\mu} + 2 d^\dagger_i d_i \right) + V \sum_{i,\sigma,\sigma'} \left(c^\dagger_{i\sigma} z_{i\sigma'\sigma} f_{i\sigma'} + h.c. \right) \\ & + \sum_i \left[U d^\dagger_i d_i + \alpha_i \left(e^\dagger_i e_i + \sum_\mu p^\dagger_{i\mu} p_{i\mu} + d^\dagger_i d_i - 1 \right) \right] \\ & + \sum_i \left[\beta_{i0} \left(\sum_\sigma f^\dagger_{i\sigma} f_{i\sigma} - \sum_\mu p^\dagger_{i\mu} p_{i\mu} - 2 d^\dagger_i d_i \right) + \vec{\beta}_i \cdot \left(\sum_{\sigma,\sigma'} f^\dagger_{i\sigma'} \vec{\tau}_{\sigma\sigma'} f_{i\sigma} - (p^\dagger_{i0} \vec{p}_i + \vec{p}_i{}^\dagger p_{i0}) \right) \right]. \end{aligned} \qquad (66)$$

An application of the SPA to this Hamiltonian describing spiral magnetic states has been considered in [71]. There, the nonmagnetic boson saddle-point amplitudes e, d, p_0 and Lagrange parameters α, β_0 have been assumed spatially uniform, while the magnetic parameters $\vec{p}_i$ and $\vec{\beta}_i$ were taken to have the spatial dependence of a spiral vector field, $\vec{p}_i = p(\cos\phi_i, \sin\phi_i, 0)$ and $\vec{\beta}_i = \beta(\cos\phi_i, \sin\phi_i, 0)$ oriented perpendicular to the $z-$axis in spin space, and $\phi_i = \vec{q}\cdot\vec{R}_i$. The spatial periodicity characterized by the wave vector $\vec{q}$ leads to a coupling of Bloch states at wave vectors $\vec{k}$ and $\vec{k}+\vec{q}$. The energy matrix of the hybridized bands then takes the form

$$\epsilon_{\vec{k}} = \begin{pmatrix} \epsilon_{\vec{k}} - \mu & V z_+ & 0 & V z_- \\ V z_+ & \epsilon_a + \beta_0 - \mu & V z_- & \beta \\ 0 & V z_- & \epsilon_{\vec{k}+\vec{q}} - \mu & V z_+ \\ V z_- & \beta & V z_+ & \epsilon_a + \beta_0 - \mu \end{pmatrix} \qquad (67)$$

where the weight factors $z_\pm$ are defined by

$$z_\pm = \frac{e p_+ + d p_-}{\sqrt{1 - d^2 - p_+^2}\,\sqrt{1 - e^2 - p_-^2}} \pm \frac{e p_- + d p_+}{\sqrt{1 - d^2 - p_-^2}\,\sqrt{1 - e^2 - p_+^2}} \qquad (68)$$

with $p_\pm = (p_0 \pm p)/\sqrt{2}$. Requiring that the free energy

$$F = -\frac{1}{\beta}\sum_{\vec{k}\sigma\alpha} \ln\left[1 + \mathrm{e}^{\frac{-E_{\vec{k}\sigma\alpha}}{T}}\right] + Ud^2 + \alpha(e^2 + p_0^2 + p^2 + d^2) - \beta_0(p_0^2 + p^2 + 2d^2) + 2\beta p_0 p \quad (69)$$

be stationary yields the saddle-point values. Here $E_{\vec{k},\sigma,\alpha}$ are the eigenvalues of the energy matrix $\epsilon_{\vec{k}}$ given in Eq. (67).

The zero-temperature phase diagram in the (t/U)-δ plane (with the t nearest-neighbor hopping amplitude and δ the filling factor of the conduction band) has been calculated in [71]. Spiral magnetic states have been found in a wide region, with wave vector $\vec{q}$ approaching the edge of the Brillouin zone at $\delta = 1$ (antiferromagnetic order). Approaching the limit $\delta = 0$, one finds a ferromagnetic region, followed by another antiferromagnetic state very close to $\delta = 0$. These findings have been confirmed by quantum Monte Carlo simulations [72]. One should keep in mind that the spatial dimension enters only through the energy dispersion of the conduction electrons. These results are therefore best applicable in three or higher dimensions, where fluctuation effects are expected to be small.

5 Fluctuation corrections to the saddle-point approximation: SRI representation of the Hubbard model

The spin and charge response functions of the Hubbard model have been considered as well. In particular, in the SRI representation they may be directly evaluated, as all degrees of freedom have been mapped onto bosons. Indeed, the spin and density fluctuations may be expressed as

$$\sum_\sigma \sigma\delta n_\sigma = \delta(p_0^\dagger p_3 + p_3^\dagger p_0) \equiv \delta S_z \quad \text{and} \quad \sum_\sigma \delta n_\sigma = \delta(d^\dagger d - e^\dagger e) \equiv \delta N. \quad (70)$$

This allows one to write the spin and charge autocorrelation functions in terms of the slave-boson correlation functions as

$$\begin{aligned} \chi_s(k) &= \sum_{\sigma,\sigma'} \sigma\sigma' \langle \delta n_\sigma(-k)\, \delta n_{\sigma'}(k)\rangle = \langle \delta S_z(-k)\, \delta S_z(k)\rangle \\ \chi_c(k) &= \sum_{\sigma\sigma'} \langle \delta n_\sigma(-k)\, \delta n_{\sigma'}(k)\rangle = \langle \delta N(-k)\, \delta N(k)\rangle\,. \end{aligned} \quad (71)$$

Performing the calculation to one-loop order, one can make use of the propagators given in the appendix of Ref. [42] to obtain

$$\begin{aligned} \chi_s(k) &= 2p_0^2\, S_{77}^{-1}(k) \\ \chi_c(k) &= 2e^2 S_{11} S^{-1}(k) - 4ed\, S_{12}^{-1}(k) + 2d^2\, S_{22}^{-1}(k)\,. \end{aligned} \quad (72)$$

It should be emphasized here that Fermi liquid behavior is obtained when considering the above $\chi_s(k)$ and $\chi_c(k)$ in the long-wavelength and low-frequency limit [73, 74]. The obtained Landau parameters involve effective interactions that differ in the spin channel and in the charge

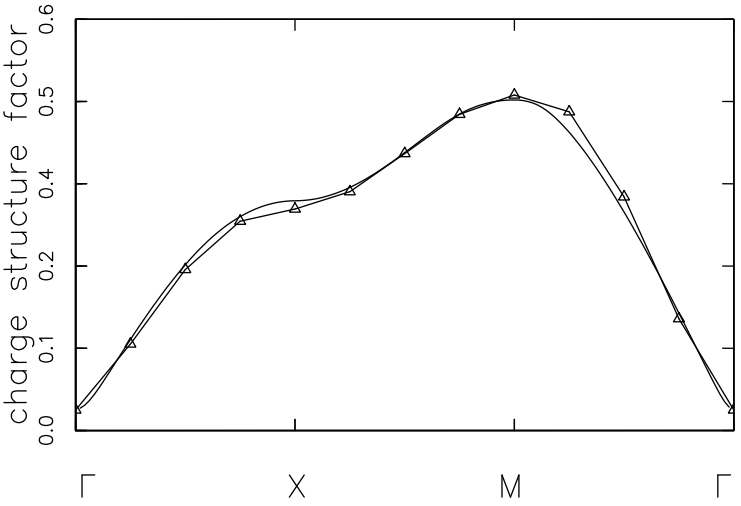

Fig. 6: *Comparison of the Quantum Monte Carlo (triangles) and Slave-Boson (full line) charge structure factors for* $U = 4\,t$*,* $\delta = 0.275$ *and* $\beta = 6/t$*.*

channel. Performing the algebra at half filling yields for a rectangular DOS

$$F_0^a = -1 + \frac{1}{(1+U/U_c)^2} \quad \text{and} \quad F_0^s = \frac{U(2U_c - U)}{(U_c - U)^2}\,. \tag{73}$$

As can be seen in Eq. (73) F_0^a remains larger than -1 when reaching the Mott transition, while F_0^s diverges (for a recent manifestation of a related behavior see [75]).

Ferromagnetic instabilities have been investigated, too [77], as well as ferromagnetic phases. In particular, in the limit $U \to \infty$, it could be shown analytically that the fully polarized ferromagnetic ground state and the paramagnetic ground state are degenerate at density $\rho = 2/3$ for any bipartite lattice [43]. For lower densities the ground state is paramagnetic.

Yet, in such an analysis, the focus is put on a ferromagnetic instability only, while other commensurate or even incommensurate instabilities should be considered as well. This analysis has been carried out for the Hubbard model on the square lattice [77]. Off half filling it turned out that the leading instabilities are systematically towards incommensurate states characterized by a wave vector (Q_x, π) for $U < 57\,t$ with Q_x smoothly varying from π for $U = 0^+$ down to 0 for $U = 57\,t$. While the Hubbard model was initially introduced, *inter alia*, to describe metallic magnetism [78, 79], this result shows that ferromagnetism is confined to the very large U regime. Further, for the largest U, the wave vector characterizing the instability is rather of the form $(0, Q_y)$, with $Q_y \simeq \pi$.

The computation of the charge structure factor has been performed, too, in particular with the aim of putting forward charge instabilities [42]. The result turned negative, even for the t-t'-U repulsive Hubbard model [80]. Instead, the charge structure factor quite systematically consists of one broad peak centered at (π, π). As an example, we compare in Fig. 6 the slave-boson result with quantum Monte Carlo simulations by Dzierzawa [81], for $U = 4\,t$ and $\delta = 0.275$ at temperature $T = t/6$. The agreement between both approaches is excellent, as the difference does not exceed a few percent.

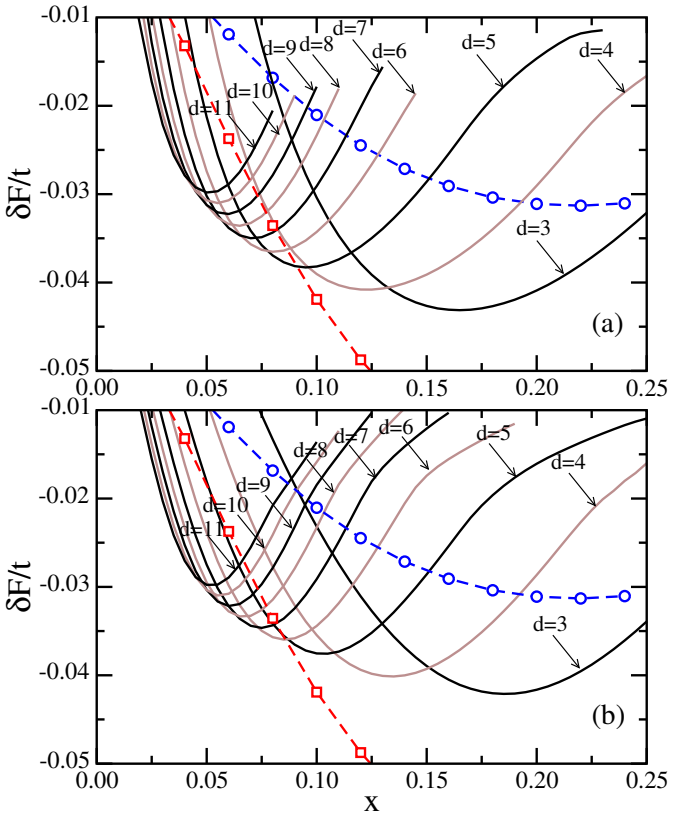

Fig. 7: *Free energy gain δF per site with respect to the AF phase as a function of doping x, obtained for the t-t'-U Hubbard Model with $U = 12\,t$ and $t' = -0.3\,t$ for: (a) Vertical site-centered striped phases; (b) vertical bond-centered striped phases. Domain walls are separated by $d = 3, \ldots, 11$ lattice constants. Circles and squares show the corresponding data for vertical and diagonal spiral order, respectively.*

5.1 Magnetic and striped phases

Since the leading instabilities of the paramagnetic phase are generally towards incommensurate phases, spiral and striped phases have been thoroughly investigated [43–46, 48–50, 57]. Comparison of ground-state energies in spiral phases with numerical simulations showed very good agreement. For instance, for $U = 4\,t$ it could be shown that the SB ground state energy is larger than its counterpart by less than 3% [44]. For larger values of U, it has been obtained that the SB ground state energy exceeds the exact diagonalization data by less than 4% (7%) for $U = 8\,t$ ($20\,t$) and doping larger than 15%. The discrepancy increases when the doping is lowered [46]. Regarding the pure Hubbard model, calculations on $L \times L$ clusters with $L > 100$ showed that magnetic striped phases are generally slightly more stable than spiral phases. However, the situation is more intricate for the t-t'-U repulsive Hubbard model. As shown in Fig. 7 for an intermediate value of t', a large number of phases compete. While the vertical site-centered striped phases are generally lower in energy than the vertical bond-centered striped phases at low doping δ, the opposite result is found at larger δ. For instance, for $U = 12\,t$, the transition occurs at $\delta \simeq 0.16$ for $t' = -0.15\,t$ and at $\delta \simeq 0.18$ for $t' = -0.3\,t$. Yet, in the latter case, the diagonal spiral phase is lower in energy for $\delta \geq 0.09$, in contrast to the former case [50].

6 Extended Hubbard model

The Hubbard model assumes a perfect screening of the long-range part of the Coulomb interaction. This may be questionable and the relevance of this approximation may be assessed by considering the extended Hubbard model that reads

$$H = \sum_{i,j,\sigma} t_{ij}\, a^\dagger_{i\sigma} a_{j\sigma} + U \sum_i \left(n_{i\uparrow} - \frac{1}{2}\right)\left(n_{i\downarrow} - \frac{1}{2}\right) + \frac{1}{2}\sum_{i,j} V_{ij}(1-n_i)(1-n_j) + \frac{1}{2}\sum_{i,j} J_{ij}\vec{S}_i \cdot \vec{S}_j\,. \tag{74}$$

It includes intersite Coulomb V_{ij} and exchange J_{ij} interactions. These elements decay fast with increasing distance $|\vec{R}_i - \vec{R}_j|$ but extend in general beyond nearest neighbors. The particle-hole symmetric form for both density-density interaction terms is consistently used.
Although one expects that $V_{ij} > 0$, in certain cases effective intersite Coulomb interactions may be attractive [82]. Therefore, $\{V_{ij}\}$ may be treated as effective parameters. Similarly, for the exchange elements $\{J_{ij}\}$ both antiferromagnetic ($J_{ij} > 0$) and ferromagnetic ($J_{ij} < 0$) exchange elements may be considered. For more details see [83].
In the SRI representation [15, 16] the Hamiltonian Eq. (74) may be represented as

$$\begin{aligned} H &= \sum_{i,j,\sigma} t_{i,j} \sum_{\sigma\sigma'\sigma_1} z^\dagger_{i\sigma_1\sigma} f^\dagger_{i\sigma} f_{j\sigma'} z_{j\sigma'\sigma_1} + U \sum_i \left(d^\dagger_i d_i - \frac{1}{2}\sum_\sigma f^\dagger_{i\sigma} f_{j\sigma'} + \frac{1}{4}\right) \\ &+ \frac{1}{4}\sum_{i,j} V_{ij}\left[\left(1 - \sum_\sigma f^\dagger_{i\sigma} f_{i\sigma}\right) Y_j + Y_i \left(1 - \sum_\sigma f^\dagger_{j\sigma} f_{j\sigma}\right)\right] \\ &+ \frac{1}{2}\sum_{i,j} J_{ij} \sum_{\sigma\sigma'\sigma_1} \vec{\tau}_{\sigma\sigma'}\, p^\dagger_{i\sigma\sigma_1} p_{i\sigma_1\sigma'} \cdot \sum_{\rho\rho'\rho_1} \vec{\tau}_{\rho\rho'}\, p^\dagger_{j\rho\rho_1} p_{j\rho_1\rho'}\,, \end{aligned} \tag{75}$$

where we used the representation of the physical quantities in terms of slave bosons Eq. (16) and expressed the hole doping operator as $Y_i \equiv e^\dagger_i e_i - d^\dagger_i d_i$.

6.1 Saddle-point approximation to the extended Hubbard model

In the paramagnetic phase the saddle-point approximation to the extended Hubbard model (74) runs in a fashion analogous to section 4.2 [83], though with the quasiparticle dispersion (Eq. (41)) modified into

$$E_{\vec{k}\sigma} = z_0^2 t_{\vec{k}} + \beta_0 - \frac{1}{2}U - \frac{1}{2}V_0 Y - \mu\,, \tag{76}$$

in which the Fourier transform of the intersite Coulomb repulsion, $V_{\vec{k}} = \frac{1}{L}\sum_{i,j} V_{ij}\, e^{-i\vec{k}\cdot(\vec{R}_j - \vec{R}_i)}$, was introduced. The steps leading to the saddle-point equations Eqs. (44) can be repeated, and the final saddle-point equation is again given by Eq. (46). We therefore obtain the remarkable result that the slave-boson mean values are independent of $\{J_{ij}\}$ and $\{V_{ij}\}$. Hence, in a paramagnetic phase, the intersite interactions only influence the fluctuations and do not change electron localization due to strong onsite interaction U. In particular, the nearest-neighbor Coulomb interaction V has no influence on the Mott gap, and the results obtained by Lavagna [35] also apply to the extended Hubbard model.

6.2 Landau parameters

In this section we present the homogenous spin and charge instabilities that are generated or magnified by the intersite Coulomb and exchange interactions. We follow the derivation of Lhoutellier *et al.* [83] and make use of the inverse propagator matrix they derived. Moreover, spin and charge fluctuations separate at the one-loop order, and the intersite Coulomb (exchange) elements have no effect on the value of F_0^a (F_0^s). We recall that a ferromagnetic (charge) instability is identified by $F_0^a = -1$ ($F_0^s = -1$).

6.2.1 Ferromagnetic instability — F_0^a parameter

Fortunately enough, an analytical expression of the Landau parameter F_0^a at half filling can be obtained. It reads

$$F_0^a = 2N_F^{(0)}\,\bar{\varepsilon}\left\{\frac{u(2+u)}{(1+u)^2} - \frac{J_0/U_c}{1-u^2}\right\}, \tag{77}$$

where we have introduced $u = U/U_c$ and the bare density of states at the Fermi energy $N_F^{(0)}$. Eq. (77) consists of a regular and a singular part. The regular part generalizes the result Eq. (73) to an arbitrary DOS. It follows from the Hubbard model and has been discussed in much detail [59, 74]. In particular, in the metallic phase at half filling, it systematically yields values of F_0^a larger than -1 for generic lattices such as the cubic lattice for which $2N_F^{(0)}\bar{\varepsilon} = -1.14$. The singular part depends solely on the $\vec{k} = 0$ component of the exchange coupling, $J_0 \equiv J_{\vec{k}=0}$ and not on the details of $\{J_{ij}\}$ [84]. It triggers a ferromagnetic (FM) instability in the metallic phase for $J_0 < 0$ regardless of its value, while it stiffens the spin response for $J_0 > 0$, as shown in Fig. 8a. We emphasize that the ferromagnetic instability deduced from Eq. (77) is general and occurs in all cases *below* the metal-to-insulator transition when $J_0 < 0$. This result follows from the band narrowing when $U \to U_c$, which amplifies the effects of the intersite exchange interaction.

The physical origin of Eq. (77) lies in the fact that, in the limit of vanishing hopping, the Hubbard model at half filling favors the formation of localized magnetic moments that order according to the exchange couplings, for instance ferromagnetically for $J_0 < 0$. Further, our result suggests that a minimum of coherence of the quasi particles z_F^2 is necessary to destabilize the ferromagnetic order. It only depends on $j_0 \equiv J_0/U$ and, for a rectangular DOS for which $2N_F^{(0)}\bar{\varepsilon} = -1$, reads

$$z_F^2 = \frac{4j_0 + j_0^2 + (1-j_0)\sqrt{1-6j_0+j_0^2} - 1}{4j_0^2}\,. \tag{78}$$

It behaves as $z_F^2 \simeq -2j_0$ for small FM exchange. Hence, for $J_0 \to 0^-$ the FM instability takes place at $U = U_c$, while it is absent for $J_0 = 0$. This is the only case for which the spin susceptibility is finite at the Brinkman-Rice point U_c. Fig. 8a shows that the location of the FM instability depends rather sensitively on the FM coupling, from U_c^- for $J = 0^+$ down to $0.33\,U_c$ for $J/U = -0.2$.

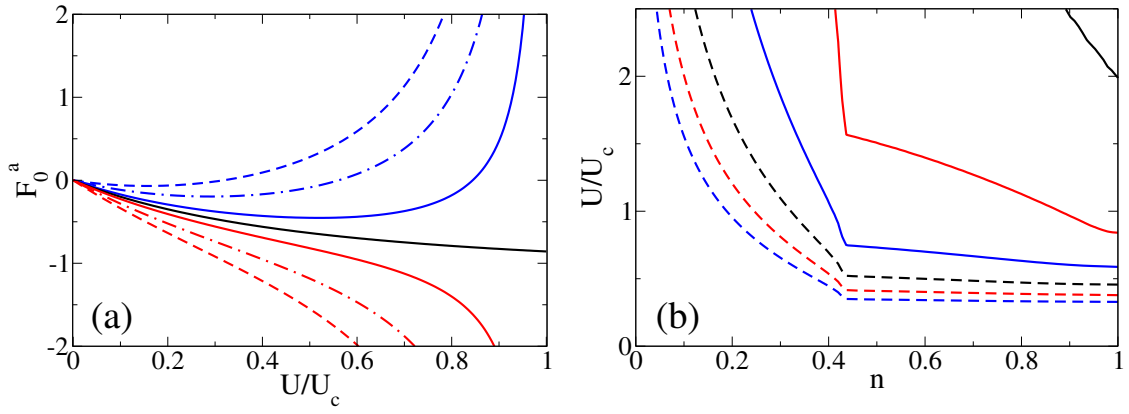

Fig. 8: *(a) Landau parameter F_0^a for the extended Hubbard model at half filling on the cubic lattice with different lines from top to bottom for decreasing $J/U = 0.2, 0.1, 0.04, 0, -0.04, -0.1, -0.2$. (b) Instability lines of the unpolarized state towards FM order as given by the divergence of the magnetic susceptibility (Landau parameter $F_0^a = -1$) for the extended Hubbard model with FM exchange $J < 0$ on the cubic lattice with different lines from top to bottom for $J/U = 0, -0.01, -0.05, -0.1, -0.15, -0.2$.*

Also, away from half filling, finite FM exchange coupling $J_0 < 0$ triggers the FM instability at significantly lower values of U. For instance, Fig. 8b shows that, in the case of the cubic lattice, $J/U = -0.01$ already brings this instability down to the values of $U \sim 20\,t$ for the doping $\delta < 0.57$ where the DOS is almost independent of energy. When $J/U = -0.05$, the FM instability occurs at $U < 10\,t$ in the same doping regime and comes down also for lower electron fillings. For lower J_0, the FM instability occurs at even lower values of U. This is in contrast to the calculations for the two-band model presented in section 4.4, where the FM instability was only found in the doped Mott insulator regime. In that case, no intersite FM coupling is needed and the FM instability follows from Hund's exchange.

On the contrary, an antiferromagnetic coupling suppresses the FM instability, and the value of $J/U = 0.1$ totally removes ferromagnetism.

6.2.2 Charge instability — F_0^s parameter

The symmetric Landau parameter F_0^s, which stands for the charge response, has to be evaluated numerically even at half filling, except for $V = 0$. As expected, F_0^s vanishes for $U = 0$, as F_0^a does. Otherwise, the symmetric parameter F_0^s increases with U in the entire regime of filling $0 < \rho \leq 1$. This increase is stronger near half filling, where $F_0^s > 10$ for $U/U_c > 0.7$ in a range of small doping away from half filling, see Fig. 9a. At half filling the value of the positive F_0^s is given by Eq. (73). It rapidly increases and finally diverges at the metal-to-insulator transition (we recall that for the simple cubic lattice $U_c \simeq 16.04\,t$). Away from $\rho = 1$, the increase of F_0^s is moderate, and it follows the same pattern as $1/z^2$ in Fig. 1, being another manifestation of strong electron correlations near half filling. The increase of F_0^s with increasing U/U_c is enhanced by a positive intersite Coulomb repulsion in the extended Hubbard model. When $V > 0$, one finds even a stronger increase of F_0^s near half filling, and finally it becomes even larger than $F_0^s = 10$ in a broad range of filling $\rho > 0.6$ for the cubic lattice at $V = 0.2\,U$. The

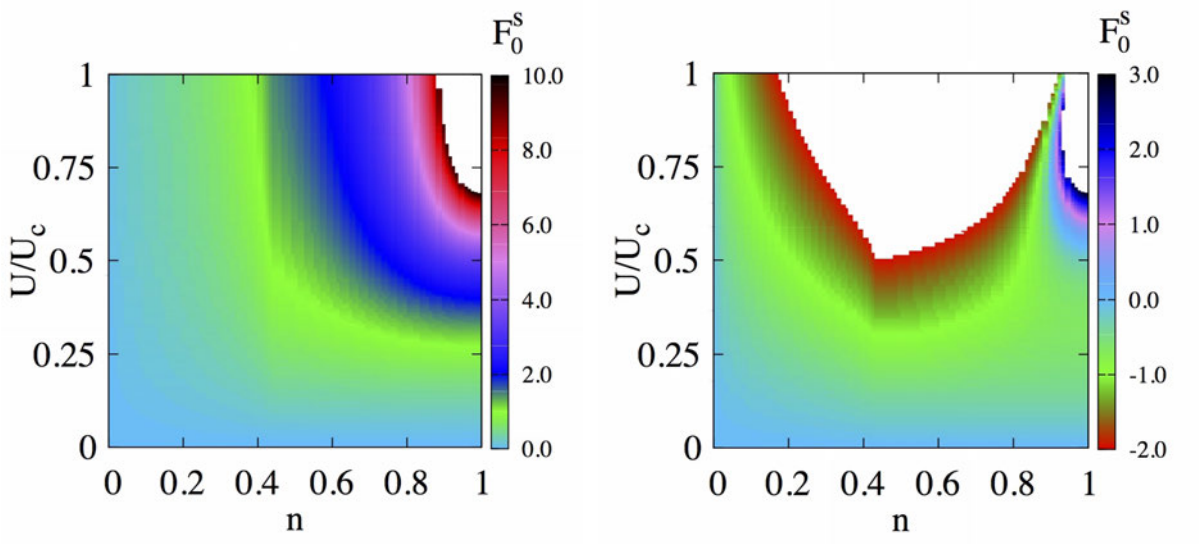

Fig. 9: *(a) Landau parameter F_0^s for the Hubbard model on the cubic lattice. Here the white region stands for values $F_0^s > 10$. No instability is found. (b) Landau parameter F_0^s for the extended Hubbard model on the cubic lattice with attractive intersite interaction $V/U = -0.2$. Large values of $F_0^s > 3$ are found only near $\rho = 1$, while the charge instability $F_0^s = -1$ occurs for a broad range of $0.045 < n < 0.93$. Note that the instability line $F_0^s = -1$ extends to $n = 1^-$, and stops at $U \simeq 1.246\, U_c$.*

uniform charge distribution is therefore more robust in the regime of $\rho \simeq 1$, if $V/U > 0$.

The uniform charge distribution is destabilized by attractive charge interactions $V < 0$, particularly in the regime near quarter filling. At $V = -0.2\,U$ the value of F_0^s decreases with increasing U for any filling ρ and this decrease is fastest near quarter filling. For $U < U_c$ one finds the charge instability at $F_0^s = -1$ in a broad range of $\rho \in (0.045, 0.93)$. This instability is related to the shape of the DOS and is easiest to realize at $\rho \simeq 0.42$, where the DOS has a van Hove singularity. Remarkably, U and V cooperate to cause this striking tendency towards phase separation that is absent for $V = 0$.

The data of Fig. 9b suggest that in the case of charge response the regime near the metal-to-insulator transition at half filling is robust and the Landau parameter F_0^s is here always enhanced, even for $V < 0$.

We now inspect the case $\rho = 1$ in more detail. It can be noticed in Fig. 10 that F_0^s is reduced for attractive V while it is enhanced for repulsive V. The reduction of F_0^s occurs only for sufficiently large $-V$ and is visible in Fig. 10 for $V/U = -0.15$, and beyond. As a result, a minimum in F_0^s develops at $U \simeq 0.4\, U_c$, the minimal value of F_0^s decreases with increasing $-V$, and a charge instability may be found at the critical value $V/U < -0.234$, see the inset in Fig. 10. The instability moves towards lower values of U with decreasing V when the minimum of F_0^s becomes deeper with further decreasing V. Particularly interesting is the non-monotonic behavior of F_0^s with increasing U for $V < 0$. We therefore suggest that a sufficiently strong intersite Coulomb attraction $-V/U > 0.234$ is necessary to induce phase separation. The instability is absent for repulsive V, where the uniform charge distribution is locally stable. The nature of the instabilities at finite wave vector is an open question.

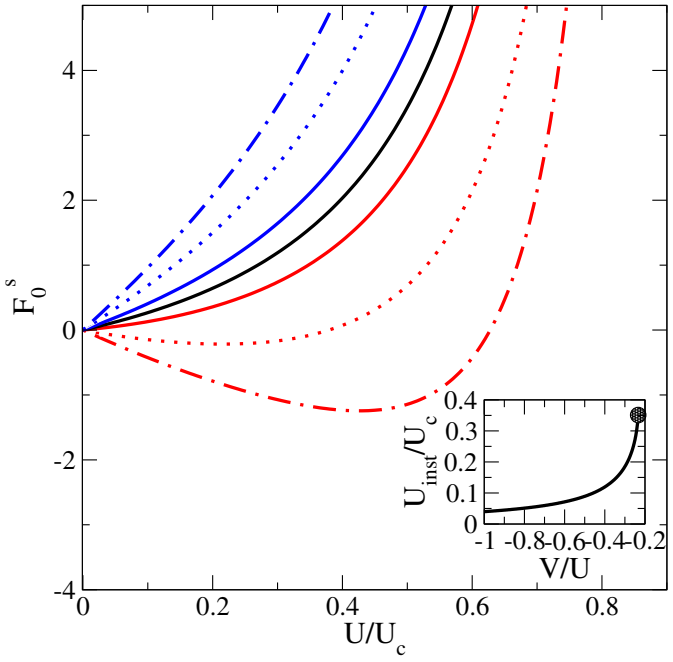

Fig. 10: *Landau parameter F_0^s for the extended Hubbard model on the cubic lattice at half filling ($\rho = 1$) for selected decreasing values of intersite Coulomb interaction V from top to bottom: $V/U{=}0$ (black line), $V/U>0$ (blue): $V/U{=}0.05$ (solid line), $V/U{=}0.15$ (dotted) and $V/U{=}0.25$ (dashed-dotted line), and $V/U<0$ (red): $V/U{=}-0.05$ (solid line), $V/U{=}-0.15$ (dotted) and $V/U{=}-0.25$ (dashed-dotted line). The inset shows the instability value $U_{\rm inst}/U_c$ for $V/U \in [-1.0,-0.2]$. Its end point is marked by a solid circle.*

7 Summary

We have reviewed the most prominent auxiliary particle techniques and their applications to strongly correlated electron systems, using a variety of approximation schemes, ranging from saddle-point approximations, possibly with Gaussian fluctuations, to exact evaluation of quantities represented in the functional integral formalism.

It has been shown how to handle the radial SB fields that appear when making use of the gauge symmetry associated to a particular SB representation to gauge away the phase degree of freedom of the SB. It was further made evident that the exact expectation value of a radial SB field is generally finite and unrelated to a Bose condensation.

It was seen that the Kotliar-Ruckenstein representation, especially in its spin-rotation invariant formulation, is particularly useful for identifying complex spin- and/or charge-ordered ground states in saddle-point approximations, since it treats all spin and charge states on a lattice site on the same footing. Regarding the Hubbard model on the square lattice, unrestricted Hartree-Fock calculations point towards a huge number of solutions. An indication that this is also realized using slave bosons on the saddle-point level is provided by Fig. 7, but identifying the numerous competing phases remains a challenge. Yet ferromagnetic ground states could only be found in the very large $U > 8\,W$ regime, as a reminiscence of Nagaoka ferromagnetism.

The Kotliar-Ruckenstein slave-boson technique has also been applied to the orbitally degener-

ate case. The main results are the following a) low-energy single-particle quantities such as the critical value of the interaction strength at which the transition occurs, the quasiparticle residue and the single-particle Mott-Hubbard gap depend very weakly on degeneracy, justifying the agreement between theory and experiment when it was applied to orbitally degenerate systems, b) the degeneracy temperature decreases with increasing band degeneracy, c) the Mott-Hubbard transition depends strongly on J_H, d) there is a coexistence region of metallic-like and insulating-like solutions of the saddle-point equations, e) ferromagnetism appears as a property of doped Mott insulators.
Results have been presented for a Hubbard model extended with long-ranged Coulomb and exchange interactions. It was shown that they have no effect on the Mott-Hubbard gap in the paramagnetic phase. Calculations of the Landau parameter F_0^s show that attractive interactions lead to charge instabilities in a broad density range away from half filling, signaling a tendency towards phase separation. The presented calculations of F_0^a predict a ferromagnetic instability in a strongly correlated metallic system with globally ferromagnetic exchange. The analytic result for F_0^a Eq. (77) uncovers that, for any lattice, the Hubbard model at half filling is on the verge of a ferromagnetic instability, which is triggered by an infinitesimal ferromagnetic intersite exchange. This result provides a new context for the original idea of Kanamori [79], who introduced the Hubbard model as the simplest model of itinerant ferromagnetism.

Acknowledgment

I am deeply indebted to Peter Wölfle and Thilo Kopp for all the enlightening discussions we had along many years that form the foundation for this review, and Klaus Doll, Michael Dzierzawa, Hans Kroha, Gabi Kotliar, Grégoire Lhoutellier, Ulrike Lüders, Burkhart Möller, Andrzej Oleś, Henni Ouerdane, Marcin Raczkowski, and Walter Zimmermann for valuable collaboration.
I gratefully acknowledge financial support by the Région Basse-Normandie and the Ministère de la Recherche.

References

[1] M. Imada, A. Fujimori, and Y. Tokura, Rev. Mod. Phys. **70**, 1039 (1998)

[2] P.A. Lee, T.M. Rice, J. Serene, L.J. Sham and J.W. Wilkins, Comments on Condensed Matter Physics, **12,** 99 (1986)

[3] J.G. Bednorz and K.A. Müller, Z. Physik B **64**, 189 (1986); B. Raveau, C. Michel, M. Hervieu, and D. Groult: *Crystal Chemistry of High-T_c Superconducting Copper Oxides*, Springer Series in Materials Science **15** (Springer, Heidelberg, 1991)

[4] P.W. Anderson, Science **235,** 1196 (1987)

[5] A.C. Hewson: *The Kondo Problem to Heavy Fermions* (Cambridge Univ. Press, 1993)

[6] R.Frésard, J.Kroha, and P.Wölfle in: *Theoretical Methods for Strongly Correlated Systems*, A. Avella and F. Mancini (eds.), Springer Series in Solid-State Sciences **171** (Springer, Heidelberg, 2012) pp. 65–101

[7] T. Holstein and H. Primakoff, Phys. Rev. **58,** 1094 (1940)

[8] J. Schwinger: *Quantum Theory of Angular Momentum*, H. Biedenharn and H. Van Dam (eds.) (Academic, New York, 1965)

[9] A.A. Abrikosov, Physics (Long Island City, N.Y.) **2**, 5 (1965)

[10] B. Coqblin and J.R. Schrieffer, Phys. Rev. **185**, 847 (1969)

[11] S.E. Barnes, J. Phys. F **6**, 1375 (1976); **7**, 2637 (1977)

[12] P. Coleman, Phys. Rev. B **29**, 3035 (1984)

[13] M. Gutzwiller, Phys. Rev. Lett. **10**, 159 (1963)

[14] G. Kotliar and A.E. Ruckenstein, Phys. Rev. Lett. **57**, 1362 (1986)

[15] T.C. Li, P. Wölfle, and P.J. Hirschfeld, Phys. Rev. B **40**, 6817 (1989)

[16] R. Frésard and P. Wölfle, Int. J. of Mod. Phys. B **6**, 685 (1992), Int. J. of Mod. Phys. B **6**, 3087 (1992)

[17] R. Frésard and G. Kotliar, Phys. Rev. B **56**, 12 909 (1997)

[18] H. Hasegawa, J. Phys. Soc. Jpn. **66**, 1391 (1997)

[19] F. Lechermann, A. Georges, G. Kotliar, and O. Parcollet, Phys. Rev. B **76**, 155102 (2007)

[20] J. Bünemann, Phys. Stat. Sol. (b) **248**, 203 (2011)

[21] R. Frésard, H. Ouerdane, and T. Kopp, Nucl. Phys. B **785**, 286 (2007)

[22] R. Frésard and T. Kopp, Ann. Phys. (Berlin) **524**, 175 (2012)

[23] C. Castellani, C.R. Nanoli and J. Ranninger, Phys. Rev. B **18**, 4945 (1978)

[24] R. von Helmolt, J. Wecker, B. Holzapfel, L. Schultz, and K. Samwer, Phys. Rev. Lett. **71**, 2331 (1993); Y. Tomioka, A. Asamitsu, Y. Moritomo, H. Kuwahara, and Y. Tokura, Phys. Rev. Lett. **74**, 5108 (1995) B. Raveau, A. Maignan, and V. Caignaert, J. Solid State Chem. **117**, 424 (1995); A. Maignan, C. Simon, V. Caignaert, and B. Raveau, Solid State Commun. **96**, 623 (1995)

[25] H. Kawazoe, H. Yasakuwa, H. Hyodo, M. Kurota, H. Yanagi, and H. Hosono, Nature **389**, 939 (1997)

[26] L. Li, C. Richter, S. Paetel, T. Kopp, J. Mannhart, and R.C. Ashoori, Science **332**, 825 (2011)

[27] H. Ohta et al, Nature Mat. **6**, 129 (2007); R. Frésard, S. Hébert, A. Maignan, L. Pi, and J. Hejtmanek, Phys. Lett. A **303**, 223 (2002); A. Maignan, C. Martin, R. Frésard, V. Eyert, E. Guilmeau, S. Hébert, M. Poienar, and D. Pelloquin, Solid State Commun. **149**, 962 (2009)

[28] N. Reyren, S. Thiel, A. D. Caviglia, L. Fitting Kourkoutis, G. Hammerl, C. Richter, C.W. Schneider, T. Kopp, A.-S. Rüetschi, D. Jaccard, M. Gabay, D.A. Muller, J.-M. Triscone, and J. Mannhart, Science **317**, 1196 (2007)

[29] V. Eyert, U. Schwingenschlögl, C. Hackenberger, T. Kopp, R. Frésard, and U. Eckern, Prog. Solid State Chem. **36**, 156 (2008)

[30] U. Lüders, W.C. Sheets, A. David, W. Prellier, and R. Frésard, Phys. Rev. B **80**, 241102(R) (2009)

[31] R. Frésard and T. Kopp, Nucl. Phys. B **594**, 769 (2001)

[32] The correctness of a particular representation may be verified through the exact evaluation of, e.g., the partition function and Green's functions in the atomic limit.

[33] N. Read, D.M. Newns, J. Phys. C **16**, L1055 (1983); *ibid.* 3273 (1983); D.M. Newns and N. Read, Adv. in Physics **36,** 799 (1987)

[34] J.W. Rasul, T. Li, J. Phys. C **21**, 5119 (1988); T.C. Li and J.W. Rasul, Phys. Rev. B **39**, 4630 (1989); J.W. Rasul, T.C. Li and H. Beck, Phys. Rev. B **39**, 4191 (1989)

[35] M. Lavagna, Phys. Rev. B **41**, 142 (1990); Helvetica Physica Acta **63**, 310 (1990); Int. J. Mod. Phys. B **5**, 885 (1991)

[36] Th. Jolicœur and J.C. Le Guillou, Phys. Rev. B **44**, 2403 (1991)

[37] Y. Bang, C. Castellani, M. Grilli, G. Kotliar, R. Raimondi and Z. Wang, Int. J. of Mod. Phys. B **6**, 531 (1992)

[38] W. Metzner, and D. Vollhardt, Phys. Rev. Lett. **62**, 324 (1989); Phys. Rev. B **37**, 7382 (1988); W. Metzner, Z. Phys. B **77**, 253 (1989)

[39] E. Müller-Hartmann, Z. Phys. B **74**, 507 (1989)

[40] J. Kroha, P. Hirschfeld, K.A. Muttalib, and P. Wölfle Solid State Comm. **83**, 1003 (1992); J. Kroha, P. Wölfle, and T.A. Costi, Phys. Rev. Lett. **79**, 261 (1997); J. Kroha and P. Wölfle, Acta Phys. Pol. B **29**, 3781 (1998); S. Kirchner and J. Kroha, J. Low Temp. Phys. **126**, 1233 (2002)

[41] R. Frésard and T. Kopp, Phys. Rev. B. **78**, 073108 (2008)

[42] W. Zimmermann, R. Frésard, and P. Wölfle, Phys. Rev. B **56**, 10 097 (1997)

[43] B. Möller, K. Doll, and R. Frésard, J. Phys. Condensed Matter **5** 4847 (1993)

[44] R. Frésard, M. Dzierzawa and P. Wölfle, Europhys. Lett. **15**, 325 (1991)

[45] E. Arrigoni and G.C. Strinati, Phys. Rev. B **44**, 7455 (1991)

[46] R. Frésard and P. Wölfle, J. Phys.: Condensed Matter **4** 3625 (1992)

[47] P.A. Igoshev, M.A. Timirgazin, A.K. Arzhnikov, and V.Y. Irkhin, JETP Lett. **98**, 150 (2013)

[48] G. Seibold, E. Sigmund, and V. Hizhnyakov, Phys. Rev. B **57**, 6937 (1998)

[49] M. Raczkowski, R. Frésard, and A.M. Oleś, Phys. Rev. B **73**, 174525 (2006)

[50] M. Raczkowski, R. Frésard, and A.M. Oleś, Europhys. Lett. **76**, 128 (2006)

[51] A. Isidori and M. Capone, Phys. Rev. B **80**, 115120 (2009)

[52] A. Ruegg, S. Pilgram, and M. Sigrist, Phys. Rev. B **75**, 195117 (2007)

[53] P. Korbel, W. Wojcik, A. Klejnberg, J. Spałek, M. Acquarone, and M. Lavagna, Eur. Phys. J. B, **32**, 315 (2003)

[54] G. Kotliar, E. Lange, and M.J. Rozenberg, Phys. Rev. Lett. **84**, 5180 (2000)

[55] G. Seibold, Phys. Rev. B **58**, 15520 (1998)

[56] N. Pavlenko and T. Kopp, Phys. Rev. Lett. **97**, 187001 (2006)

[57] J. Lorenzana and G. Seibold, Low Temp. Phys. **32**, 320 (2006)

[58] W.F. Brinkman and T.M. Rice, Phys. Rev. B. **2**, 4302 (1970)

[59] D. Vollhardt, Rev. Mod. Phys. **56**, 99 (1984);
D. Vollhardt, P. Wölfle, and P.W. Anderson, Phys. Rev. B. **35**, 6703 (1987)

[60] M.J. Rozenberg *et al*, Phys. Rev. Lett. **75**, 105 (1995)

[61] R. Frésard and K. Doll, Proceedings of the NATO ARW *The Hubbard Model: Its Physics and Mathematical Physics*, D. Baeriswyl, D.K. Campbell, J.M.P. Carmelo, F. Guinea, and E. Louis (eds.), San Sebastian, 1993 (Plenum Press, 1995), p. 385

[62] C. Noce and M. Cuoco, Phys. Rev. B **59**, 2659 (1999)

[63] R. Frésard and M. Lamboley, J. Low Temp. Phys. **126**, 1091 (2002)

[64] D. Vollhardt, N. Blümer, K. Held, M. Kollar, J. Schlimpf, and M. Ulmke,
Z. Phys. B **103**, 283 (1997)

[65] H.C. Nguyen and J.B. Goodenough, Phys. Rev. B **52**, 8776 (1995)

[66] M. Imada, A. Fujimori, and Y. Tokura, Rev. Mod. Phys. **70**, 1039 (1998)

[67] G. Cao, S. McCall, V. Dobrosavljevic, C.S. Alexander, J.E. Crow, and R.P. Guertin,
Phys. Rev. B **61**, R5053 (2000)

[68] C. Schuster, U. Lüders, R. Frésard, and U. Schwingenschlögl, EPL **103**, 37003 (2012)

[69] S. Doniach, Physica B&C **91**, 231 (1977)

[70] H. v. Löhneysen, A. Rosch, M. Vojta and P. Wölfle, Rev. Mod. Phys. **79**, 1015 (2007)

[71] B. Möller and P. Wölfle, Phys. Rev. B **48**, 10320 (1993)

[72] M. Guerrero and R.M. Noack, Phys. Rev. B **53**, 3707 (1996)

[73] T.C. Li, Y.S. Sun and P. Wölfle, Z. Phys. B – Condensed Matter **82**, 369 (1991)

[74] T.C. Li and P. Bénard, Phys. Rev. B. **50**, 17 387 (1994)

[75] P. Limelette, H. Muguerra, and S. Hébert, Phys. Rev. B **82**, 035123 (2010)

[76] J.P. Lu, Phys. Reb. B **49**, 5687 (1994)

[77] K. Doll, M. Dzierzawa, R. Frésard, and P. Wölfle,
Z. Phys. B – Condensed Matter **90**, 297 (1993)

[78] J. Hubbard, Proc. R. Soc. London A **276**, 238 (1963)

[79] J. Kanamori, Prog. Theor. Phys. **30**, 275 (1963)

[80] R. Frésard and W. Zimmermann, Phys. Rev. B **58**, 15288 (1998)

[81] M. Dzierzawa, unpublished

[82] R. Micnas, J. Ranninger, and S. Robaszkiewicz, Rev. Mod. Phys. B **62**, 113 (1990)

[83] G. Lhoutellier, R. Frésard, and A.M. Oleś, Phys. Rev. B **91**, 224410 (2015)

[84] In the specific case of J_{ij} restricted to nearest neighbor on the cubic lattice one has $J_0 = 6J$.